DeepMDP: Learning Continuous Latent Space Models for Representation Learning

Carles Gelada [1]   Saurabh Kumar [1]   Jacob Buckman [2]   Ofir Nachum [1]   Marc G. Bellemare [1]

Abstract

Many reinforcement learning (RL) tasks provide the agent with high-dimensional observations that can be simplified into low-dimensional continuous states. To formalize this process, we introduce the concept of a *DeepMDP*, a parameterized latent space model that is trained via the minimization of two tractable losses: prediction of rewards and prediction of the distribution over next latent states. We show that the optimization of these objectives guarantees (1) the quality of the latent space as a representation of the state space and (2) the quality of the DeepMDP as a model of the environment. We connect these results to prior work in the bisimulation literature, and explore the use of a variety of metrics. Our theoretical findings are substantiated by the experimental result that a trained DeepMDP recovers the latent structure underlying high-dimensional observations on a synthetic environment. Finally, we show that learning a DeepMDP as an auxiliary task in the Atari 2600 domain leads to large performance improvements over model-free RL.

1. Introduction

In reinforcement learning (RL), it is typical to model the environment as a Markov Decision Process (MDP). However, for many practical tasks, the state representations of these MDPs include a large amount of redundant information and task-irrelevant noise. For example, image observations from the Arcade Learning Environment (Bellemare et al., 2013) consist of 33,600-dimensional pixel arrays, yet it is intuitively clear that there exist lower-dimensional approximate representations for all games. Consider PONG; observing only the positions and velocities of the three objects in the frame is enough to play. Converting each frame into such a simplified state before learning a policy facilitates the learning process by reducing the redundant and irrelevant information presented to the agent. Representation learning techniques for reinforcement learning seek to improve the learning efficiency of existing RL algorithms by doing exactly this: learning a mapping from states to simplified states.

Prior work on representation learning, such as state aggregation with bisimulation metrics (Givan et al., 2003; Ferns et al., 2004; 2011) or feature discovery algorithms (Comanici & Precup, 2011; Mahadevan & Maggioni, 2007; Bellemare et al., 2019), has resulted in algorithms with good theoretical properties; however, these algorithms do not scale to large scale problems or are not easily combined with deep learning. On the other hand, many recently-proposed approaches to representation learning via deep learning have strong empirical results on complex domains, but lack formal guarantees (Jaderberg et al., 2016; van den Oord et al., 2018; Fedus et al., 2019). In this work, we propose an approach to representation learning that unifies the desirable aspects of both of these categories: a deep-learning-friendly approach with theoretical guarantees.

We describe the *DeepMDP*, a latent space model of an MDP which has been trained to minimize two tractable losses: predicting the rewards and predicting the distribution of next latent states. DeepMDPs can be viewed as a formalization of recent works which use neural networks to learn latent space models of the environment (Ha & Schmidhuber, 2018; Oh et al., 2017; Hafner et al., 2018; Francois-Lavet et al., 2018), because the value functions in the DeepMDP are guaranteed to be good approximations of value functions in the original task MDP. To provide this guarantee, careful consideration of the metric between distribution is necessary. A novel analysis of Maximum Mean Discrepancy (MMD) metrics (Gretton et al., 2012) defined via a function norm allows us to provide such guarantees; this includes the Total Variation, the Wasserstein and Energy metrics. These results represent a promising first step towards principled latent-space model-based RL algorithms.

From the perspective of representation learning, the state of a DeepMDP can be interpreted as a representation of the

---

[1]Google Brain [2]Center for Language and Speech Processing, Johns Hopkins University. Correspondence to: Carles Gelada <cgel@google.com>.
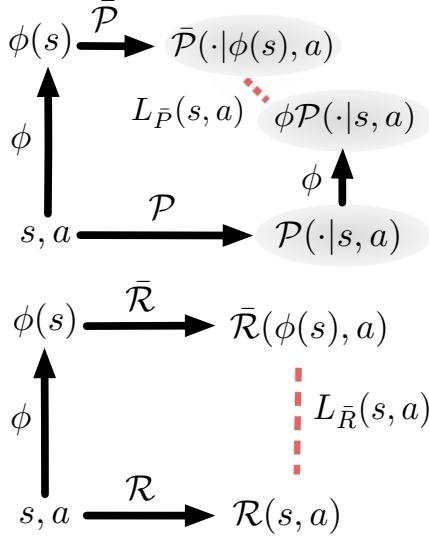
Figure 1. Diagram of the latent space losses. Circles denote a distribution.

original MDP's state. When the Wasserstein metric is used for the latent transition loss, analysis reveals a profound theoretical connection between DeepMDPs and bisimulation. These results provide a theoretically-grounded approach to representation learning that is salable and compatible with modern deep networks.

In Section 2, we review key concepts and formally define the DeepMDP. We start by studying the model-quality and representation-quality results of DeepMDPs (using the Wasserstein metric) in Sections 3 and 4. In Section 5, we investigate the connection between DeepMDPs using the Wasserstein and bisimulation. Section 6 generalizes *only* our model-based guarantees to metrics other than the Wasserstein; this limitation emphasizes the special role of that the Wasserstein metric plays in learning good representations. Finally, in Section 8 we consider a synthetic environment with high-dimensional observations and show that a Deep-MDP learns to recover its underlying low-dimensional latent structure. We then demonstrate that learning a DeepMDP as an auxiliary task to model-free RL in the Atari 2600 environment leads to significant improvement in performance when compared to a baseline model-free method.

2. Background

2.1. Markov Decision Processes

Define a Markov Decision Process (MDP) in standard fashion: $\mathcal{M} = \langle \mathcal{S}, \mathcal{A}, \mathcal{R}, \mathcal{P}, \gamma \rangle$ (Puterman, 1994). For simplicity of notation we will assume that $\mathcal{S}$ and $\mathcal{A}$ are discrete spaces unless otherwise stated. A policy π defines a distribution over actions conditioned on the state, $\pi(a|s)$. Denote

by Π the set of all stationary policies. The value function of a policy $\pi \in \Pi$ at a state s is the expected sum of future discounted rewards by running the policy from that state. $V^\pi : \mathcal{S} \to \mathbb{R}$ is defined as:

$$V^\pi(s) = \underset{\substack{a_t \sim \pi(\cdot|s_t) \\ s_{t+1} \sim \mathcal{P}(\cdot|s_t, a_t)}}{\mathbb{E}} \left[\sum_{t=0}^\infty \gamma^t \mathcal{R}(s_t, a_t) | s_0 = s \right].$$

The action value function is similarly defined:

$$Q^\pi(s, a) = \underset{\substack{a_t \sim \pi(\cdot|s_t) \\ s_{t+1} \sim \mathcal{P}(\cdot|s_t, a_t)}}{\mathbb{E}} \left[\sum_{t=0}^\infty \gamma^t \mathcal{R}(s_t, a_t) | s_0 = s, a_0 = a \right]$$

We denote by $\mathcal{P}_{\bar{\pi}}$ the action-independent transition function induced by running a policy π, $\mathcal{P}_{\bar{\pi}}(s'|s) = \sum_{a \in \mathcal{A}} \mathcal{P}(s'|s, a)\pi(a|s)$. Similarly $\mathcal{R}_{\bar{\pi}}(s) = \sum_{a \in \mathcal{A}} \mathcal{R}(s, a)\pi(a|s)$. We denote π^* as the optimal policy in $\mathcal{M}$; i.e., the policy which maximizes expected future reward. We denote the optimal state and action value functions with respect to π^* as V^*, Q^*. We denote the stationary distribution of a policy π in $\mathcal{M}$ by ξ_π; i.e.,

$$\xi_\pi(s) = \sum_{\dot{s} \in \mathcal{S}, \dot{a} \in \mathcal{A}} \mathcal{P}(s|\dot{s}, \dot{a})\pi(\dot{a}|\dot{s})\xi_\pi(\dot{s})$$

We overload notation by also denoting the state-action stationary distribution as $\xi_\pi(s, a) = \xi_\pi(s)\pi(a|s)$. Although only non-terminating MDPs have stationary distributions, a state distribution for terminating MDPs with similar properties exists (Gelada & Bellemare, 2019).

2.2. Latent Space Models

For some MDP $\mathcal{M}$, let $\overline{\mathcal{M}} = \langle \bar{\mathcal{S}}, \mathcal{A}, \bar{\mathcal{R}}, \bar{\mathcal{P}}, \gamma \rangle$ be an MDP where $\bar{\mathcal{S}}$ is a continuous space with metric $d_{\bar{\mathcal{S}}}$ and a shared action space $\mathcal{A}$ between $\mathcal{M}$ and $\overline{\mathcal{M}}$. Furthermore, let $\phi : \mathcal{S} \to \bar{\mathcal{S}}$ be an embedding function which connects the state spaces of these two MDPs. We refer to $(\overline{\mathcal{M}}, \phi)$ as a *latent space model* of $\mathcal{M}$.

Since $\overline{\mathcal{M}}$ is, by definition, an MDP, value functions can be defined in the standard way. We use $\bar{V}^{\bar{\pi}}, \bar{Q}^{\bar{\pi}}$ to denote the value functions of a policy $\bar{\pi} \in \bar{\Pi}$, where $\bar{\Pi}$ is the set of policies defined on the state space $\bar{\mathcal{S}}$. The transition and reward functions, $\bar{\mathcal{R}}_{\bar{\pi}}$ and $\bar{\mathcal{P}}_{\bar{\pi}}$, of a policy $\bar{\pi}$ are also defined in the standard manner. We use $\bar{\pi}^*$ to denote the optimal policy in $\overline{\mathcal{M}}$. The corresponding optimal state and action value functions are then $\bar{V}^*, \bar{Q}^*$. For ease of notation, when $s \in \mathcal{S}$, we use $\bar{\pi}(\cdot|s) := \bar{\pi}(\cdot|\phi(s))$ to denote first using ϕ to map s to the state space $\bar{\mathcal{S}}$ of $\overline{\mathcal{M}}$ and subsequently using $\bar{\pi}$ to generate the probability distribution over actions.

Although similar definitions of latent space models have been previously studied (Francois-Lavet et al., 2018; Zhang et al., 2018; Ha & Schmidhuber, 2018; Oh et al., 2017;

Hafner et al., 2018; Kaiser et al., 2019; Silver et al., 2017), the parametrizations and training objectives used to learn such models have varied widely. For example Ha & Schmidhuber (2018); Hafner et al. (2018); Kaiser et al. (2019) use pixel prediction losses to learn the latent representation while (Oh et al., 2017) chooses instead to optimize the model to predict next latent states with the same value function as the sampled next states.

In this work, we study the minimization of loss functions defined with respect to rewards and transitions in the latent space:

$$L_{\bar{\mathcal{R}}}(s,a) = |\mathcal{R}(s,a) - \bar{\mathcal{R}}(\phi(s),a)| \tag{1}$$

$$L_{\bar{\mathcal{P}}}(s,a) = \mathcal{D}\left(\phi\mathcal{P}(\cdot|s,a), \bar{\mathcal{P}}(\cdot|\phi(s),a)\right) \tag{2}$$

where we use the shorthand notation $\phi\mathcal{P}(\cdot|s,a)$ to denote the probability distribution over $\bar{\mathcal{S}}$ of first sampling $s' \sim \mathcal{P}(\cdot|s,a)$ and then embedding $\bar{s}' = \phi(s')$, and where $\mathcal{D}$ is a metric between probability distributions. To provide guarantees, $\mathcal{D}$ in Equation 2 needs to be chosen carefully. For the majority of this work, we focus on the Wasserstein metric; in Section 6, we generalize some of the results to alternative metrics from the Maximum Mean Discrepancy family. Francois-Lavet et al. (2018) and Chung et al. (2019) have considered similar latent losses, but to the best of our knowledge ours is the first theoretical analysis of these models. See Figure 1 for an illustration of how the latent space losses are constructed.

We use the term *DeepMDP* to refer to a parameterized latent space model trained via the minimization of losses consisting of $L_{\bar{\mathcal{R}}}$ and $L_{\bar{\mathcal{P}}}$ (sometimes referred to as *DeepMDP losses*). In Section 3, we derive theoretical guarantees of DeepMDPs when minimizing $L_{\bar{\mathcal{R}}}$ and $L_{\bar{\mathcal{P}}}$ over the whole state space. However, our principal objective is to learn DeepMDPs parameterized by deep networks, which requires DeepMDP losses in the form of expectations; we show in Section 4 that similar theoretical guarantees can be obtained in this setting.

2.3. Wasserstein Metric

Initially studied in the optimal transport literature (Villani, 2008), the Wasserstein-1 (which we simply refer to as the Wasserstein) metric $W_d(P,Q)$ between two distributions P and Q, defined on a space with metric d, corresponds to the minimum cost of transforming P into Q, where the cost of moving a particle at point x to point y comes from the underlying metric $d(x,y)$.

Definition 1. *The Wasserstein-1 metric W between distributions P and Q on a metric space $\langle \chi, d \rangle$ is:*

$$W_d(P,Q) = \inf_{\lambda \in \Gamma(P,Q)} \int_{\chi \times \chi} d(x,y)\lambda(x,y)\, dx\, dy.$$

where $\Gamma(P,Q)$ denotes the set of all couplings of P and Q.

When there is no ambiguity on what the underlying metric d is, we will simply write W. The Monge-Kantorovich duality (Mueller, 1997) shows that the Wasserstein has a dual form:

$$W_d(P,Q) = \sup_{f \in \mathcal{F}_d} |\mathbb{E}_{x \sim P} f(x) - \mathbb{E}_{y \sim Q} f(y)|, \tag{3}$$

where $\mathcal{F}_d$ is the set of 1-Lipschitz functions under the metric d, $\mathcal{F}_d = \{f : |f(x) - f(y)| \leqslant d(x,y)\}$.

2.4. Lipschitz Norm of Value Functions

The degree to which a value function of $\overline{\mathcal{M}}$, $\bar{V}^{\bar{\pi}}$ approximates the value function V^{π} of $\mathcal{M}$ will depend on the Lipschitz norm of $\bar{V}^{\bar{\pi}}$. In this section we define and provide conditions for value functions to be Lipschitz.[1] Note that we study the Lipschitz properties of DeepMDPs $\overline{\mathcal{M}}$ (instead of a MDP $\mathcal{M}$) because in this work, only the Lipschiz properties of DeepMDPs are relevant; the reader should note that these results follow for any continuous MDP with a metric state space.

We say a policy $\bar{\pi} \in \bar{\Pi}$ is *Lipschitz-valued* if its value function is Lipschitz, i.e. it has Lipschitz $\bar{Q}^{\bar{\pi}}$ and $\bar{V}^{\bar{\pi}}$ functions.

Definition 2. *Let $\overline{\mathcal{M}}$ be a DeepMDP with a metric $d_{\bar{\mathcal{S}}}$. A policy $\bar{\pi} \in \bar{\Pi}$ is $K_{\bar{V}}$-Lipschitz-valued if for all $\bar{s}_1, \bar{s}_2 \in \bar{\mathcal{S}}$:*

$$\left|\bar{V}^{\bar{\pi}}(\bar{s}_1) - \bar{V}^{\bar{\pi}}(\bar{s}_2)\right| \leqslant K_{\bar{V}} d_{\bar{\mathcal{S}}}(\bar{s}_1, \bar{s}_2),$$

and if for all $a \in \mathcal{A}$:

$$\left|\bar{Q}^{\bar{\pi}}(\bar{s}_1, a) - \bar{Q}^{\bar{\pi}}(\bar{s}_2, a)\right| \leqslant K_{\bar{V}} d_{\bar{\mathcal{S}}}(\bar{s}_1, \bar{s}_2).$$

Several works have studied Lipschitz norm constraints on the transition and reward functions (Hinderer, 2005; Asadi et al., 2018) to provide conditions for value functions to be Lipschitz. Closely following their formulation, we define Lipschitz DeepMDPs as follows:

Definition 3. *Let $\overline{\mathcal{M}}$ be a DeepMDP with a metric $d_{\bar{\mathcal{S}}}$. We say $\overline{\mathcal{M}}$ is $(K_{\bar{\mathcal{R}}}, K_{\bar{\mathcal{P}}})$-Lipschitz if, for all $\bar{s}_1, \bar{s}_2 \in \bar{\mathcal{S}}$ and $a \in \mathcal{A}$:*

$$\left|\bar{\mathcal{R}}(\bar{s}_1, a) - \bar{\mathcal{R}}(\bar{s}_2, a)\right| \leqslant K_{\bar{\mathcal{R}}} d_{\bar{\mathcal{S}}}(\bar{s}_1, \bar{s}_2)$$
$$W\left(\bar{\mathcal{P}}(\cdot|, \bar{s}_1, a), \bar{\mathcal{P}}(\cdot|\bar{s}_2, a)\right) \leqslant K_{\bar{\mathcal{P}}} d_{\bar{\mathcal{S}}}(\bar{s}_1, \bar{s}_2)$$

From here onwards, we will we restrict our attention to the set of Lipschitz DeepMDPs for which the constant $K_{\bar{\mathcal{P}}}$ is sufficiently small, formalized in the following assumption:

Assumption 1. *The Lipschitz constant $K_{\bar{\mathcal{P}}}$ of the transition function $\bar{\mathcal{P}}$ is strictly smaller than $\frac{1}{\gamma}$.*

---

[1] Another benefit of MDP smoothness is improved learning dynamics. Pirotta et al. (2015) suggest that the smaller the Lipschitz constant of an MDP, the faster it is to converge to a near-optimal policy.

From a practical standpoint, Assumption 1 is relatively strong, but simplifies our analysis by ensuring that close states cannot have future trajectories that are "divergent." An MDP might still not exhibit divergent behaviour even when $K_{\overline{\mathcal{P}}} \geqslant \frac{1}{\gamma}$. In particular, when episodes terminate after a finite amount of time, Assumption 1 becomes unnecessary. We leave as future work how to improve on this assumption.

We describe a small set of Lipschitz-valued policies. For any policy $\bar{\pi} \in \overline{\Pi}$, we refer to the Lipschitz norm of its transition function $\overline{\mathcal{P}}_{\bar{\pi}}$ as $K_{\mathcal{P}_{\bar{\pi}}} \geqslant W\left(\overline{\mathcal{P}}_{\bar{\pi}}(\cdot|\bar{s}_1), \overline{\mathcal{P}}_{\bar{\pi}}(\cdot|\bar{s}_2)\right)$ for all $\bar{s}_1, \bar{s}_2 \in \mathcal{S}$. Similarly, we denote the Lipschitz norm of the reward function as $K_{\overline{\mathcal{R}}_{\bar{\pi}}} \geqslant |\overline{\mathcal{R}}_{\bar{\pi}}(\bar{s}_1) - \overline{\mathcal{R}}_{\bar{\pi}}(\bar{s}_2)|$.

Lemma 1. *Let $\overline{\mathcal{M}}$ be $(K_{\overline{\mathcal{R}}}, K_{\overline{\mathcal{P}}})$-Lipschitz. Then,*

1. *The optimal policy $\bar{\pi}^*$ is $\frac{K_{\overline{\mathcal{R}}}}{1-\gamma K_{\overline{\mathcal{P}}}}$-Lipschitz-valued.*

2. *All policies with $K_{\overline{\mathcal{P}}_{\bar{\pi}}} \leqslant \frac{1}{\gamma}$ are $\frac{K_{\overline{\mathcal{R}}_{\bar{\pi}}}}{1-\gamma K_{\overline{\mathcal{P}}_{\bar{\pi}}}}$-Lipschitz-valued.*

3. *All constant policies (i.e. $\bar{\pi}(a|\bar{s}_1) = \bar{\pi}(a|\bar{s}_2), \forall a \in \mathcal{A}, \bar{s}_1, \bar{s}_2 \in \overline{\mathcal{S}})$ are $\frac{K_{\overline{\mathcal{R}}}}{1-\gamma K_{\overline{\mathcal{P}}}}$-Lipschitz-valued.*

Proof. See Appendix A for all proofs. $\square$

A more general framework for understanding Lipschitz value functions is still lacking. Little prior work studying classes of Lipschitz-valued policies exists in the literature and we believe that this is an important direction for future research.

3. Global DeepMDP Bounds

We now present our first main contributions: concrete DeepMDP losses, and several bounds which provide us with useful guarantees when these losses are minimized. We refer to these losses as the *global* DeepMDP losses, to emphasize their dependence on the whole state and action space:[2]

$$L_{\mathcal{R}}^{\infty} = \sup_{s \in \mathcal{S}, a \in \mathcal{A}} |\mathcal{R}(s,a) - \overline{\mathcal{R}}(\phi(s),a)| \quad (4)$$

$$L_{\mathcal{P}}^{\infty} = \sup_{s \in \mathcal{S}, a \in \mathcal{A}} W\left(\phi\mathcal{P}(\cdot|s,a), \overline{\mathcal{P}}(\cdot|\phi(s),a)\right) \quad (5)$$

3.1. Value Difference Bound

We start by bounding the difference of the value functions $Q^{\bar{\pi}}$ and $\overline{Q}^{\bar{\pi}}$ for any policy $\bar{\pi} \in \overline{\Pi}$. Note that $Q^{\bar{\pi}}(s,a)$ is computed using $\mathcal{P}$ and $\mathcal{R}$ on $\mathcal{S}$ while $\overline{Q}^{\bar{\pi}}(\phi(s),a)$ is computed using $\overline{\mathcal{P}}$ and $\overline{\mathcal{R}}$ on $\overline{\mathcal{S}}$.

Lemma 2. *Let $\mathcal{M}$ and $\overline{\mathcal{M}}$ be an MDP and DeepMDP respectively, with an embedding function ϕ and global loss*

---

[2]The ∞ notation is a reference to the ℓ_∞ norm

functions $L_{\mathcal{R}}^{\infty}$ and $L_{\mathcal{P}}^{\infty}$. For any $K_{\overline{V}}$-Lipschitz-valued policy $\bar{\pi} \in \overline{\Pi}$ the value difference can be bounded by

$$\left|Q^{\bar{\pi}}(s,a) - \overline{Q}^{\bar{\pi}}(\phi(s),a)\right| \leqslant \frac{L_{\mathcal{R}}^{\infty} + \gamma K_{\overline{V}} L_{\mathcal{P}}^{\infty}}{1-\gamma},$$

The previous result holds for all policies $\overline{\Pi} \subseteq \Pi$, a subset of all possible policies Π. The reader might ask whether this is an interesting set of policies to consider; in Section 5, we answer with a fat "yes" by characterizing this set via a connection with bisimulation.

A bound similar to Lemma 2 can be found in Asadi et al. (2018), who study non-latent transition models using the Wasserstein metric when there is access to an exact reward function. We also note that our results are arguably simpler, since we do not require the treatment of MDP transitions in terms of distributions over a set of deterministic components.

3.2. Representation Quality Bound

When a representation is used to predict the value of a policy in $\mathcal{M}$, a clear failure case is when two states with different values are collapsed to the same representation. The following result demonstrates that when the global DeepMDP losses $L_{\mathcal{R}}^{\infty} = 0$ and $L_{\mathcal{P}}^{\infty} = 0$, this failure case can never occur for the embedding function ϕ.

Theorem 1. *Let $\mathcal{M}$ and $\overline{\mathcal{M}}$ be an MDP and DeepMDP respectively, let $d_{\overline{\mathcal{S}}}$ be a metric in $\overline{\mathcal{S}}$, ϕ be an embedding function and $L_{\mathcal{R}}^{\infty}$ and $L_{\mathcal{P}}^{\infty}$ be the global loss functions. For any $K_{\overline{V}}$-Lipschitz-valued policy $\bar{\pi} \in \overline{\Pi}$ the representation ϕ guarantees that for all $s_1, s_2 \in \mathcal{S}$ and $a \in \mathcal{A}$,*

$$\left|Q^{\bar{\pi}}(s_1,a) - Q^{\bar{\pi}}(s_2,a)\right| \leqslant K_{\overline{V}} d_{\overline{\mathcal{S}}}(\phi(s_1), \phi(s_2))$$
$$+ 2\frac{L_{\mathcal{R}}^{\infty} + \gamma K_{\overline{V}} L_{\mathcal{P}}^{\infty}}{1-\gamma}$$

This result justifies learning a DeepMDP and using the embedding function ϕ as a representation to predict values. A similar connection between the quality of representations and model based objectives in the linear setting was made by Parr et al. (2008).

3.3. Suboptimality Bound

For completeness, we also bound the performance loss of running the optimal policy of $\overline{\mathcal{M}}$ in $\mathcal{M}$, compared to the optimal policy π^*. See Theorem 5 in Appendix A.

4. Local DeepMDP Bounds

In large-scale tasks, data from many regions of the state space is often unavailable,[3] making it infeasible to measure – let alone optimize – the global losses. Further, when the capacity of a model is limited, or when sample efficiency is a concern, it might not even be desirable to precisely learn a model of the whole state space. Interestingly, we can still provide similar guarantees based on the DeepMDP losses, as measured under an *expectation* over a state-action distribution, denoted here as ξ. We refer to these as the losses *local* to ξ. Taking $L_{\bar{\mathcal{R}}}^{\xi}$, $L_{\bar{\mathcal{P}}}^{\xi}$ to be the reward and transition losses under ξ, respectively, we have the following local DeepMDP losses:

$$L_{\bar{\mathcal{R}}}^{\xi} = \mathop{\mathbb{E}}_{s,a\sim\xi} |\mathcal{R}(s,a) - \bar{\mathcal{R}}(\phi(s),a)|, \tag{6}$$

$$L_{\bar{\mathcal{P}}}^{\xi} = \mathop{\mathbb{E}}_{s,a\sim\xi} \left[W\left(\phi\mathcal{P}(\cdot|s,a), \bar{\mathcal{P}}(\cdot|\phi(s),a)\right)\right]. \tag{7}$$

Losses of this form are compatible with the stochastic gradient decent methods used by neural networks. Thus, study of the local losses allows us to bridge the gap between theory and practice.

4.1. Value Difference Bound

We provide a value function bound for the local case, analogous to Lemma 2.

Lemma 3. *Let $\mathcal{M}$ and $\overline{\mathcal{M}}$ be an MDP and DeepMDP respectively, with an embedding function ϕ. For any $K_{\bar{V}}$-Lipschitz-valued policy $\bar{\pi} \in \bar{\Pi}$, the expected value function difference can be bounded using the local loss functions $L_{\bar{\mathcal{R}}}^{\xi_{\bar{\pi}}}$ and $L_{\bar{\mathcal{P}}}^{\xi_{\bar{\pi}}}$ measured under $\xi_{\bar{\pi}}$, the stationary state action distribution of $\bar{\pi}$.*

$$\mathop{\mathbb{E}}_{s,a\sim\xi_{\bar{\pi}}} \left|Q^{\bar{\pi}}(s,a) - \bar{Q}^{\bar{\pi}}(\phi(s),a)\right| \leqslant \frac{L_{\bar{\mathcal{R}}}^{\xi_{\bar{\pi}}} + \gamma K_{\bar{V}} L_{\bar{\mathcal{P}}}^{\xi_{\bar{\pi}}}}{1-\gamma},$$

The provided bound guarantees that for any policy $\bar{\pi} \in \bar{\Pi}$ which visits state-action pairs (s,a) where $L_{\bar{\mathcal{R}}}(s,a)$ and $L_{\bar{\mathcal{P}}}(s,a)$ are small, the DeepMDP will provide accurate value functions for any states likely to be seen under the policy.[4]

4.2. Representation Quality Bound

We can also extend the local value difference bound to provide a local bound on how well the representation ϕ can be used to predict the value function of a policy $\bar{\pi} \in \bar{\Pi}$, analogous to Theorem 1.

---

[3]Challenging exploration environments like Montezuma's Revenge are a prime example.

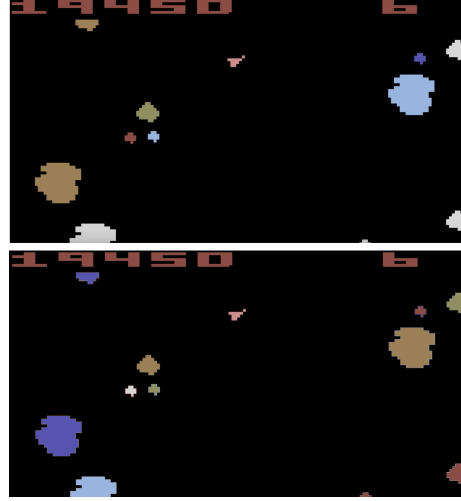[4]The value functions might be inaccurate in states that the policy $\bar{\pi}$ rarely visits.

Figure 2. A pair of bisimilar states. In the game of ASTEROIDS, the colors of the asteroids can vary randomly, but this in no way impacts gameplay.

Theorem 2. *Let $\mathcal{M}$ and $\overline{\mathcal{M}}$ be an MDP and DeepMDP respectively, let $d_{\bar{\mathcal{S}}}$ be the metric in $\bar{\mathcal{S}}$ and ϕ be the embedding function. Let $\bar{\pi} \in \bar{\Pi}$ be any $K_{\bar{V}}$-Lipschitz-valued policy with stationary distribution $\xi_{\bar{\pi}}$, and let $L_{\bar{\mathcal{R}}}^{\xi_{\bar{\pi}}}$ and $L_{\bar{\mathcal{P}}}^{\xi_{\bar{\pi}}}$ be the local loss functions. For any two states $s_1, s_2 \in \mathcal{S}$, the representation ϕ is such that,*

$$|V^{\bar{\pi}}(s_1) - V^{\bar{\pi}}(s_2)| \leqslant K_{\bar{V}} d_{\bar{\mathcal{S}}}(\phi(s_1), \phi(s_2))$$
$$+ \frac{L_{\bar{\mathcal{R}}}^{\xi_{\bar{\pi}}} + \gamma K_{\bar{V}} L_{\bar{\mathcal{P}}}^{\xi_{\bar{\pi}}}}{1-\gamma} \left(\frac{1}{d_{\bar{\pi}}(s_1)} + \frac{1}{d_{\bar{\pi}}(s_2)} \right)$$

Thus, the representation quality argument given in 3.2 holds for any two states s_1 and s_2 which are visited often by a policy $\bar{\pi}$.

5. Bisimulation

5.1. Bisimulation Relations

Bisimulation relations in the context of RL (Givan et al., 2003), are a formalization of behavioural equivalence between states.

Definition 4 (Givan et al. (2003))**.** *Given an MDP $\mathcal{M}$, an equivalence relation B between states is a bisimulation relation if for all states $s_1, s_2 \in \mathcal{S}$ that are equivalent under B (i.e. $s_1 B s_2$), the following conditions hold for all actions $a \in \mathcal{A}$.*

$$R(s_1, a) = R(s_2, a)$$
$$\mathcal{P}(G|s_1, a) = \mathcal{P}(G|s_2, a), \forall G \in \mathcal{S}/B$$

Where $\mathcal{S}/B$ denotes the partition of $\mathcal{S}$ under the relation B, the set of all groups of equivalent states, and where $\mathcal{P}(G|s,a) = \sum_{s'\in G} \mathcal{P}(s'|s,a)$.

Note that bisimulation relations are not unique. For example, the equality relation $=$ is always a bisimulation relation. Of particular interest is the maximal bisimulation relation $\sim$, which defines the partition $\mathcal{S}/\sim$ with the fewest elements (or equivalently, the relation that generates the largest possible groups of states). We will say that two states are bisimilar if they are equivalent under $\sim$. Essentially, two states are bisimilar if (1) they have the same immediate reward for all actions and (2) both of their distributions over next-states contain states which themselves are bisimilar. Figure 2 gives an example of states that are bisimilar in the Atari 2600 game ASTEROIDS. An important property of bisimulation relations is that any two bisimilar states s_1, s_2 must have the same optimal value function $Q^*(s_1, a) = Q^*(s_2, a), \forall a \in \mathcal{A}$. Bisimulation relations were first introduced for state aggregation (Givan et al., 2003), which is a form of representation learning, since merging behaviourally equivalent states does not result in the loss of information necessary for solving the MDP.

5.2. Bisimulation Metrics

A drawback of bisimulation relations is their *all-or-nothing* nature. Two states that are nearly identical, but differ slightly in their reward or transition functions, are treated as though they were just as unrelated as two states with nothing in common. Relying on the optimal transport perspective of the Wasserstein, Ferns et al. (2004) introduced bisimulation metrics, which are pseudometrics that quantify the behavioural similarity of two discrete states.

A pseudometric d satisfies all the properties of a metric except *identity of indiscernibles*, $d(x, y) = 0 \Leftrightarrow x = y$. A pseudometric can be used to define an equivalence relation by saying that two points are equivalent if they have zero distance; this is called the kernel of the pseudometric. Note that pseudometrics must obey the triangle inequality, which ensures the kernel satisfies the associative property. Without any changes to its definition, the Wasserstein metric can be extended to spaces $\langle \chi, d \rangle$, where d is a pseudometric. Intuitively, the usage of a pseudometric in the Wasserstein can be interpreted as allowing different points $x_1 \neq x_2$ in χ to be equivalent under the pseudometric (i.e. $d(x_1, x_2) = 0$). Thus, there is no need for transportation from one to the other.

An extension of bisimulation metrics based on Banach fixed points by Ferns et al. (2011) which allows the metric to be defined for MDPs with discrete and continuous state spaces.

Definition 5 (Ferns et al. (2011)). *Let $\mathcal{M}$ be an MDP and denote by Z the space of pseudometrics on the space $\mathcal{S}$ s.t. $d(s_1, s_2) \in [0, \infty)$ for $d \in Z$. Define the operator $F : Z \to Z$ to be:*

$$F_d(s_1, s_2) = \max_a (1 - \gamma) |\mathcal{R}(s_1, a) - \mathcal{R}(s_2, a)| + \gamma W_d(\mathcal{P}(\cdot|s_1, a), \mathcal{P}(\cdot|s_2, a)).$$

Then:

1. *The operator F is a contraction with a unique fixed point denoted by $\widetilde{d}$.*

2. *The kernel of $\widetilde{d}$ is the maximal bisimulation relation $\sim$. (i.e. $\widetilde{d}(s_1, s_2) = 0 \iff s_1 \sim s_2$)*

A useful property of bisimulation metrics is that the optimal value function difference between any two states can be upper bounded by the bisimulation metric between the two states.

$$|V^*(s_1) - V^*(s_2)| \leqslant \frac{\widetilde{d}(s_1, s_2)}{1 - \gamma}$$

Bisimulation metrics have been used for state aggregation (Ferns et al., 2004; Ruan et al., 2015), feature discovery (Comanici & Precup, 2011) and transfer learning between MDPs (Castro & Precup, 2010), but due to their high computational cost and poor compatibility with deep networks they have not been successfully applied to large scale settings.

5.3. Connection with DeepMDPs

The representation ϕ learned by global DeepMDP losses with the Wasserstein metric can be connected to bisimulation metrics.

Theorem 3. *Let $\mathcal{M}$ be an MDP and $\overline{\mathcal{M}}$ be a $K_{\overline{\mathcal{R}}}$-$K_{\overline{\mathcal{P}}}$-Lipschitz DeepMDP with metric $d_{\overline{\mathcal{S}}}$. Let ϕ be the embedding function and $L_{\overline{\mathcal{P}}}^{\infty}$ and $L_{\overline{\mathcal{R}}}^{\infty}$ be the global DeepMDP losses. The bisimulation distance in $\mathcal{M}$, $\widetilde{d} : \mathcal{S} \times \mathcal{S} \to \mathbb{R}^+$ can be upperbounded by the ℓ_2 distance in the embedding and the losses in the following way:*

$$\widetilde{d}(s_1, s_2) \leqslant \frac{(1 - \gamma)K_{\mathcal{R}}}{1 - \gamma K_{\overline{\mathcal{P}}}} d_{\overline{\mathcal{S}}}(\phi(s_1), \phi(s_2))$$
$$+ 2\left(L_{\overline{\mathcal{R}}}^{\infty} + \gamma L_{\overline{\mathcal{P}}}^{\infty} \frac{K_{\overline{\mathcal{R}}}}{1 - \gamma K_{\overline{\mathcal{P}}}}\right)$$

This result provides a similar bound to Theorem 1, except that instead of bounding the value difference $|\overline{V}^{\overline{\pi}}(s_1) - \overline{V}^{\overline{\pi}}(s_2)|$ the bisimulation distance $\widetilde{d}(s_1, s_2)$ is bounded. We speculate that similar results should be possible based on *local* DeepMDP losses, but they would require a generalization of bisimulation metrics to the local setting.

5.4. Characterizing $\overline{\overline{\Pi}}$

In order to better understand the set of policies $\overline{\overline{\Pi}}$ (which appears in the bounds of Sections 3 and 4), we

first consider the set of *bisimilar policies*, defined as $\widetilde{\Pi} = \{\pi : \forall s_1, s_2 \in \mathcal{S}, s_1 \sim s_2 \Leftrightarrow \pi(a|s_1) = \pi(a|s_2) \forall a\}$, which contains all policies that act the same way on states that are bisimilar. Although this set excludes many policies in Π, we argue that it is adequately expressive, since any policy that acts differently on states that are bisimilar is fundamentally uninteresting.[5]

We show a connection between deep policies and bisimilar policies by proving that the set of *Lipschitz-deep policies*, $\bar{\Pi}_K \subset \bar{\Pi}$, approximately contains the set of *Lipschitz-bisimilar policies*, $\widetilde{\Pi}_K \subset \widetilde{\Pi}$, defined as follows:

$$\bar{\Pi}_K = \left\{ \bar{\pi} : \forall s_1 \neq s_2 \in \mathcal{S}, \frac{|\bar{\pi}(a|s_1) - \bar{\pi}(a|s_2)|}{d_{\bar{\mathcal{S}}}(\phi(s_1), \phi(s_2))} \leqslant K \right\},$$

$$\widetilde{\Pi}_K = \left\{ \pi : \forall s_1 \neq s_2 \in \mathcal{S}, \frac{|\pi(a|s_1) - \pi(a|s_2)|}{\widetilde{d}(s_1, s_2)} \leqslant K \right\}.$$

The following theorem proves that minimizing the global DeepMDP losses ensures that for any $\widetilde{\pi} \in \widetilde{\Pi}_K$, there is a deep policy $\bar{\pi} \in \bar{\Pi}_{CK}$ which is close to $\widetilde{\pi}$, where the constant $C = \frac{(1-\gamma)K_{\bar{\mathcal{R}}}}{1 - \gamma K_{\bar{\mathcal{P}}}}$.

Theorem 4. *Let $\mathcal{M}$ be an MDP and $\overline{\mathcal{M}}$ be a $(K_{\bar{\mathcal{R}}}, K_{\bar{\mathcal{P}}})$-Lipschitz DeepMDP, with an embedding function ϕ and global loss functions $L_{\bar{\mathcal{R}}}^{\infty}$ and $L_{\bar{\mathcal{P}}}^{\infty}$. Denote by $\widetilde{\Pi}_K$ and $\bar{\Pi}_K$ the sets of Lipschitz-bisimilar and Lipschitz-deep policies. Then for any $\widetilde{\pi} \in \widetilde{\Pi}_K$ there exists a $\bar{\pi} \in \bar{\Pi}_{CK}$ which is close to $\widetilde{\pi}$ in the sense that, for all $s \in \mathcal{S}$ and $a \in \mathcal{A}$,*

$$|\widetilde{\pi}(a|s) - \bar{\pi}(a|s)| \leqslant L_{\bar{\mathcal{R}}}^{\infty} + \gamma L_{\bar{\mathcal{P}}}^{\infty} \frac{K_{\bar{\mathcal{R}}}}{1 - \gamma K_{\bar{\mathcal{P}}}}$$

6. Beyond the Wasserstein

Interestingly, value difference bounds (Lemmas 2 and 3) can be derived for many different choices of probability metric $\mathcal{D}$ (in the DeepMDP transition loss function, Equation 2). Here, we generalize the result to a family of *Maximum Mean Discrepancy (MMD)* metrics (Gretton et al., 2012) defined via a function norm that we denote as *Norm Maximum Mean Discrepancy (Norm-MMD)* metrics. Interestingly, the role of the Lipschitz norm in the value difference bounds is a consequence of using the Wasserstein; when we switch from the Wasserstein to another metric, it is replaced by a different term. We interpret these terms as different forms of smoothness of the value functions in $\overline{\mathcal{M}}$.

By choosing a metric whose associated smoothness corresponds well to the environment, we can potentially improve the tightness of the bounds. For example, in environments with highly non-Lipschitz dynamics, it may be impossible to

learn an accurate DeepMDP whose deep value function has a small Lipschitz norm. Instead, the associated smoothness of another metric might be more appropriate. Another reason to consider other metrics is computational; the Wasserstein has high computational cost and suffers from biased stochastic gradient estimates (Bikowski et al., 2018; Bellemare et al., 2017b), so minimizing a simpler metric, such as the KL, may be more convenient.

6.1. Norm Maximum Mean Discrepancy Metrics

MMD metrics (Gretton et al., 2012) are a family of probability metrics, each generated via a class of functions. They have also been studied by Müller (1997) under the name of Integral Probability Metrics.

Definition 6 (Gretton et al. (2012) Definition 2)**.** *Let P and Q be distributions on a measurable space χ and let $\mathcal{F}_{\mathcal{D}}$ be a class of functions $f : \chi \to \mathbb{R}$. The Maximum Mean Discrepancy $\mathcal{D}$ is*

$$\mathcal{D}(P, Q) = \sup_{f \in \mathcal{F}_{\mathcal{D}}} | \underset{x \sim P}{\mathbb{E}} f(x) - \underset{y \sim Q}{\mathbb{E}} f(y)|.$$

When $P = Q$ it's obvious that $\mathcal{D}(P, Q) = 0$ regardless of the function class $\mathcal{F}_{\mathcal{D}}$. But the class of functions leads to MMD metrics with different behaviours and properties. Of interest to us are function classes generated via function seminorms[6]. Concretely, we define a Norm-MMD metric $\mathcal{D}$ to be an MMD metric generated from a function class $\mathcal{F}_D$ of the following form:

$$\mathcal{F}_{\mathcal{D}} = \{f : \|f\|_{\mathcal{D}} \leqslant 1\}.$$

where $\|\cdot\|_{\mathcal{D}}$ is the *associated function seminorm* of $\mathcal{D}$. We will see that the family of Norm-MMDs are well suited for the task of latent space modeling. Their key property is the following: let $\mathcal{D}$ be a Norm-MMD, then for any function f s.t. $\|f\|_{\mathcal{D}} \leqslant K$,

$$| \underset{x \sim P}{\mathbb{E}} f(x) - \underset{y \sim Q}{\mathbb{E}} f(y)| \leqslant K \cdot \mathcal{D}(P, Q). \qquad (8)$$

We now discuss three particularly interesting examples of Norm-MMD metrics.

Total Variation: Defined as $TV(P, Q) = \frac{1}{2} \int_{\chi} |P(x) - Q(x)| \, dx$, the Total Variation is one of the most widely-studied metrics. Pinsker's inequality (Borwein & Lewis, 2005, p.63) bounds the TV with the Kullback–Leibler (KL) divergence. The Total Variation is also the Norm-MMD generated from the set of functions with absolute value bounded by 1 (Müller, 1997). Thus, the function norm $\|f\|_{TV} = \|f\|_{\infty} = \sup_{x \in \chi} |f(x)|$.

Wasserstein metric: The interpretation of the Wasserstein as an MMD metrics is clear from its dual form (Equation 3),
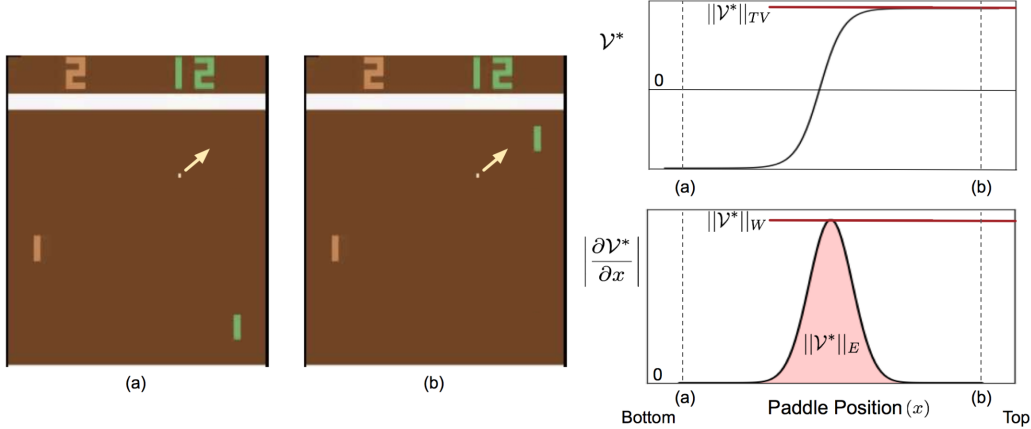

Figure 3. Visualization of the way in which different smoothness properties on the value function are derived. The left compares two near-identical frames of PONG, (a) and (b), whose only difference is the position of the player's paddle. The plots on the right show the optimal value of the state (top) and the derivative of the optimal value (bottom) as a function of the position of the player's paddle, assuming all other features of the state are kept constant. The associated smoothness of each Norm-MMD metric is shown visually. (Note that this is for illustrative purposes only, and was not actually computed from the real game. The curve in the value function represents noisy dynamics, such as those induced by "sticky actions" (Mnih et al., 2015); if the environment were deterministic, the optimal value would be a step function.)

where the function class $\mathcal{F}_W$ is set of 1-Lipschitz functions,

$$\mathcal{F}_W = \{f : |f(x) - f(y)| \leq d(x, y), \forall x, y \in \chi\}.$$

The norm associated with the Wasserstein metric $\|f\|_W$ is therefore the Lipschitz norm, which in turn is the the the ℓ_∞ norm of f' (the derivative of f). Thus, $\|f\|_W = \|f'\|_\infty = \sup_{x \in \chi} \frac{df(x)}{dx}$.

Energy distance: The energy distance E was first developed to compare distributions in high dimensions via a two sample test (Székely & Rizzo, 2004; Gretton et al., 2012). It is defined as:

$$E(P, Q) = 2 \mathop{\mathbb{E}}_{(x,y) \sim P \times Q} \|x - y\|$$
$$- \mathop{\mathbb{E}}_{x,x' \sim P} \|x - x'\| - \mathop{\mathbb{E}}_{y,y' \sim Q} \|y - y'\|,$$

where $x, x' \sim P$ denotes two independent samples of the distribution P. Sejdinovic et al. (2013) showed the connection between the energy distance and MMD metrics. Similarly to the Wasserstein, the Energy distance's associated seminorm is: $\|f\|_E = \|f'\|_1 = \int_\chi |\frac{df(x)}{dx}| \, dx$.

6.2. Value Function Smoothness

In the context of value functions, we interpret the function seminorms associated with Norm-MMD metrics as different forms of *smoothness*.

Definition 7. *Let $\bar{\mathcal{M}}$ be a DeepMDP and let $\mathcal{D}$ be a Norm-MMD with associated norm $\|\cdot\|_{\mathcal{D}}$. We say that a policy*

$\bar{\pi} \in \bar{\Pi}$ *is $K_{\bar{V}}$-smooth-valued if:*

$$\|\bar{V}^{\bar{\pi}}\|_{\mathcal{D}} \leq K_{\bar{V}}.$$

and if for all $a \in \mathcal{A}$:

$$\|\bar{Q}^{\bar{\pi}}(\cdot, a)\|_{\mathcal{D}} \leq K_{\bar{V}}.$$

For a value function $\bar{V}^{\bar{\pi}}$, $\|\bar{V}^{\bar{\pi}}\|_{TV}$ is the maximum absolute value of $\bar{V}^{\bar{\pi}}$. Both $\|\bar{V}^{\bar{\pi}}\|_W$ and $\|\bar{V}^{\bar{\pi}}\|_E$ depend on the derivative of $\bar{V}^{\bar{\pi}}$, but while $\|\bar{V}^{\bar{\pi}}\|_W$ is governed by point of maximal change, $\|\bar{V}^{\bar{\pi}}\|_E$ instead measures the amount of change over the whole state space $\bar{s}$. Thus, a value function with a small region of high derivative (and thus, large $\|\bar{V}^{\bar{\pi}}\|_W$) can still have small $\|\bar{V}^{\bar{\pi}}\|_E$. In Figure 3 we provide an intuitive visualization of these three forms of smoothness in the game of Pong.

One advantage of the Total Variation is that it requires minimal assumptions on the DeepMDP. If the reward function is bounded, i.e. $|\bar{\mathcal{R}}(\bar{s}, a)| \leq K_{\bar{\mathcal{R}}}, \forall \bar{s} \in \bar{\mathcal{S}}, a \in \mathcal{A}$, then all policies $\bar{\pi} \in \bar{\Pi}$ are $\frac{K_{\bar{\mathcal{R}}}}{1-\gamma}$-smooth-valued. We leave it to future work to study value function smoothness more generally for different Norm-MMD metrics and their associated norms.

6.3. Generalized Value Difference Bounds

The global and local value difference results (Lemmas 2 and 3), as well as the suboptimality result Lemma 1, can easily be derived when $\mathcal{D}$ is any Norm-MMD metric. Due to the repetitiveness of these results, we don't include them in the main paper; refer to Appendix A.6 for the full

statements and proofs. We leave it to future work to characterize the of policies $\bar{\bar{\Pi}}$ when general (i.e. non-Wasserstein) Norm-MMD metrics are used.

The fact that the representation quality results (Theorems 1 and 2) and the connection with bisimulation (Theorems 3 and 4) don't generalize to Norm-MMD metrics emphasizes the special role the Wasserstein metric plays for representation learning.

7. Related Work in Representation Learning

State aggregation methods (Abel et al., 2017; Li et al., 2006; Singh et al., 1995; Givan et al., 2003; Jiang et al., 2015; Ruan et al., 2015) attempt to reduce the dimensionality of the state space by joining states together, taking the perspective that a good representation is one that reduces the total number of states without sacrificing any necessary information. Other representation learning approaches take the perspective that an optimal representation contains features that allow for the linear parametrization of the optimal value function (Comanici & Precup, 2011; Mahadevan & Maggioni, 2007). Recently, Bellemare et al. (2019); Dadashi et al. (2019) approached the representation learning problem from the perspective that a good representation is one that allows the prediction via a linear map of any value function in the value function space. In contrast, we have argued that a good representation (1) allows for the parametrization of a large set of *interesting* policies and (2) allows for the good approximation of the *value function* of these policies.

Concurrently, a suite of methods combining model-free deep reinforcement learning with auxiliary tasks has shown large benefits on a wide variety of domains (Jaderberg et al., 2016; van den Oord et al., 2018; Mirowski et al., 2017). Distributional RL (Bellemare et al., 2017a), which was not initially introduced as a representation learning technique, has been shown by Lyle et al. (2019) to only play an auxiliary task role. Similarly, (Fedus et al., 2019) studied different discounting techniques by learning the spectrum of value functions for different discount values γ, and incidentally found that to be a highly useful auxiliary task. Although successful in practice, these auxiliary task methods currently lack strong theoretical justification. Our approach also proposes to minimize losses as an auxilliary task for representation learning, for a specifc choice of losses: the DeepMDP losses. We have formally justified this choice of losses, by providing theoretical guarantees on representation quality.

8. Empirical Evaluation

Our results depend on minimizing losses in expectation, which is the main requirement for deep networks to be applicable. Still, two main obstacles arise when turning
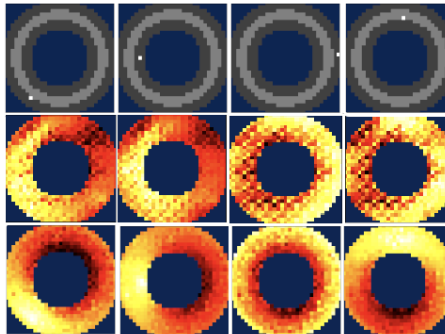
(a) One-track DonutWorld.
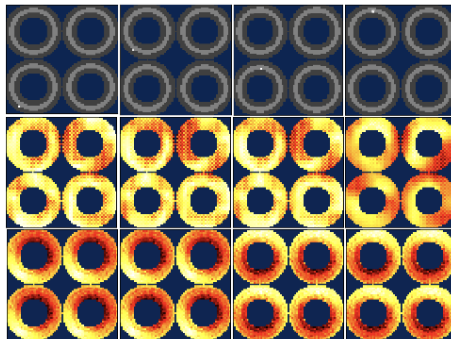
(b) Four-track DonutWorld.

Figure 4. Given a state in our DonutWorld environment (first row), we plot a heatmap of the distance between that latent state and each other latent state, for both autoencoder representations (second row) and DeepMDP representations (third row). More-similar latent states are represented by lighter colors.

these theoretical results into practical algorithms:

(1) Minimization of the Wasserstein Arjovsky et al. (2017) first proposed the use of the Wasserstein distance for Generative Adversarial Networks (GANs) via its dual formulation (see Equation 3). Their approach consists of training a network, constrained to be 1-Lipschitz, to attain the supremum of the dual. Once this supremum is attained, the Wasserstein can be minimized by differentiating through the network. Quantile regression has been proposed as an alternative solution to the minimization of the Wasserstein (Dabney et al., 2018b), (Dabney et al., 2018a), and has shown to perform well for Distributional RL. The reader might note that issues with the stochastic minimization of the Wasserstein distance have been found to be biased by Bellemare et al. (2017b) and Bikowski et al. (2018). In our experiments, we circumvent these issues by assuming that both $\mathcal{P}$ and $\bar{\mathcal{P}}$ are deterministic. This reduces the Wasserstein distance $W_{d_{\bar{\mathcal{S}}}}(\phi \mathcal{P}(\cdot|s,a), \bar{\mathcal{P}}(\cdot|\phi(s),a))$ to $d_{\bar{\mathcal{S}}}(\phi(\mathcal{P}(s,a)), \bar{\mathcal{P}}(\phi(s),a))$, where $\mathcal{P}(s,a)$ and $\bar{\mathcal{P}}(\bar{s},a)$ denote the deterministic transition functions.

(2) Control the Lipschitz constants $K_{\bar{\mathcal{R}}}$ and $K_{\bar{\mathcal{P}}}$. We also turn to the field of Wasserstein GANs for approaches to con-
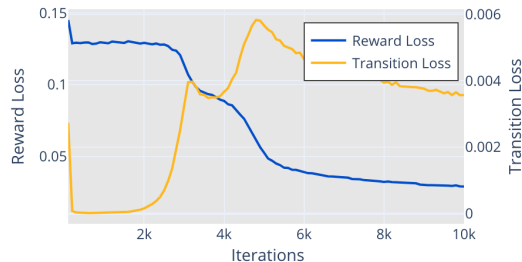
Figure 5. Due to the competition between reward and transition losses, the optimization procedure spends significant time in local minima early on in training. It eventually learns a good representation, which it then optimizes further. (Note that the curves use different scaling on the y-axis.)

strain deep networks to be Lipschitz. Originally, Arjovsky et al. (2017) used a projection step to constraint the discriminator function to be 1-Lipschitz. Gulrajani et al. (2017a) proposed using a gradient penalty, and sowed improved learning dynamics. Lipschitz continuity has also been proposed as a regularization method by Gouk et al. (2018), who provided an approach to compute an upper bound to the Lipschitz constant of neural nets. In our experiments, we follow Gulrajani et al. (2017a) and utilize the gradient penalty.

8.1. DonutWorld Experiments

In order to evaluate whether we can learn effective representations, we study the representations learned by Deep-MDPs in a simple synthetic environment we call *Donut-World*. DonutWorld consists of an agent rewarded for running clockwise around a fixed track. Staying in the center of the track results in faster movement. Observations are given in terms of 32x32 greyscale pixel arrays, but there is a simple 2D latent state space (the x-y coordinates of the agent). We investigate whether the x-y coordinates are correctly recovered when learning a two-dimensional representation.

This task epitomizes the low-dimensional dynamics, high-dimensional observations structure typical of Atari 2600 games, while being sufficiently simple to experiment with. We implement the DeepMDP training procedure using Tensorflow and compare it to a simple autoencoder baseline. See Appendix B for a full environment specification, experimental setup, and additional experiments. Code for replicating all experiments is included in the supplementary material.

In order to investigate whether the learned representations learned correspond well to reality, we plot a heatmap of closeness of representation for various states. Figure 4(a) shows that the DeepMDP representations effectively recover the underlying state of the agent, i.e. its 2D position, from

the high-dimensional pixel observations. In contrast, the autoencoder representations are less meaningful, even when the autoencoder solves the task near-perfectly.

In Figure 4(b), we modify the environment: rather than a single track, the environment now has four identical tracks. The agent starts in one uniformly at random and cannot move between tracks. The DeepMDP hidden state correctly merges all states with indistinguishable value functions, learning a deep state representation which is almost completely invariant to which track the agent is in.

The DeepMDP training loss can be difficult to optimize, as illustrated in Figure 5. This is due to the tendency of the transition and reward losses to compete with one another. If the deep state representation is uniformly zero, the transition loss will be zero as well; this is an easily-discovered local optimum, and gradient descent tends to arrive at this point early on in training. Of course, an informationless representation results in a large reward loss. As training progresses, the algorithm incurs a small amount of transition loss in return for a large decrease in reward loss, resulting in a net decrease in loss.

In DonutWorld, which has very simple dynamics, gradient descent is able to discover a good representation after only a few thousand iterations. However, in complex environments such as Atari, it is often much more difficult to discover representations that allow us to escape the low-information local minima. Using architectures with good inductive biases can help to combat this, as shown in Section 8.3. This issue also motivates the use of auxiliary losses (such as value approximation losses or reconstruction losses), which may help guide the optimizer towards good solutions; see Appendix C.5.

8.2. Atari 2600 Experiments

In this section, we demonstrate practical benefits of approximately learning a DeepMDP in the Arcade Learning Environment (Bellemare et al., 2013). Our results on *representation-similarity* indicate that learning a DeepMDP is a principled method for learning a high-quality representation. Therefore, we minimize DeepMDP losses as an auxiliary task alongside model-free reinforcement learning, learning a single representation which is shared between both tasks. Our implementations of the proposed algorithms are based on Dopamine (Castro et al., 2018).

We adopt the Distributional Q-learning approach to model-free RL; specifically, we use as a baseline the C51 agent (Bellemare et al., 2017a), which estimates probability masses on a discrete support and minimizes the KL divergence between the estimated distribution and a target distribution. C51 encodes the input frames using a convolutional neural network $\phi : \mathcal{S} \rightarrow \bar{\mathcal{S}}$, outputting a dense
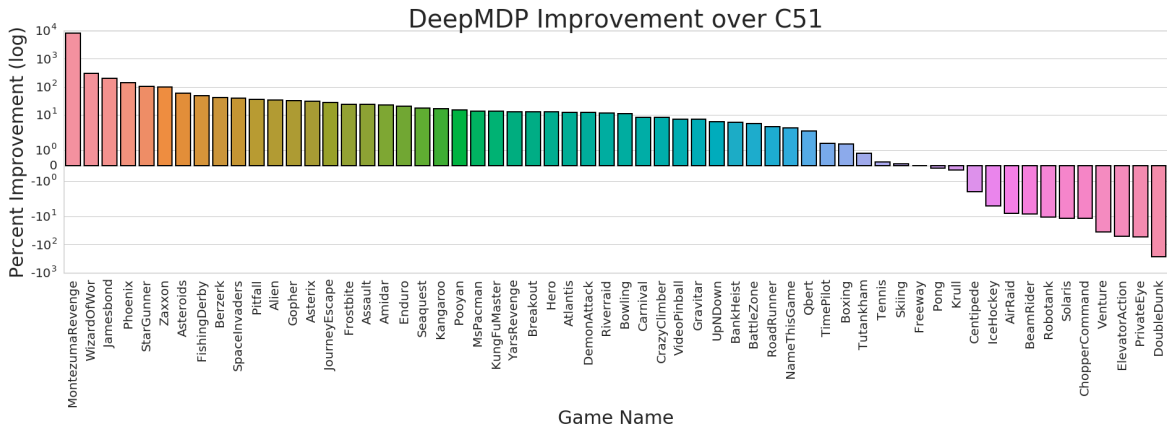
Figure 6. We compare the DeepMDP agent versus the C51 agent on the 60 games from the ALE (3 seeds each). For each game, the percentage performance improvement of DeepMDP over C51 is recorded.
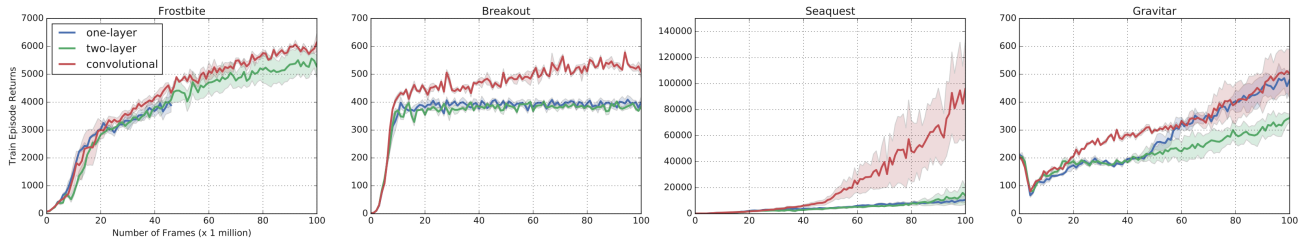

Figure 7. Performance of C51 with model-based auxiliary objectives. Three types of transition models are used for predicting next latent states: a single convolutional layer (convolutional), a single fully-connected layer (one-layer), and a two-layer fully-connected network (two-layer).

vector representation $\overline{s} = \phi(s)$. The C51 Q-function is a feed-forward neural network which maps $\overline{s}$ to an estimate of the reward distribution's logits.

To incorporate learning a DeepMDP as an auxiliary learning objective, we define a deep reward function and deep transition function. These are each implemented as a feed-forward neural network, which uses $\overline{s}$ to estimate the immediate reward and the next-state representation, respectively. The overall objective function is a simple linear combination of the standard C51 loss and the Wasserstein distance-based approximations to the local DeepMDP loss given by Equations 6 and 7. For experimental details, see Appendix C.

By optimizing ϕ to jointly minimize both C51 and Deep-MDP losses, we hope to learn meaningful $\overline{s}$ that form the basis for learning good value functions. In the following subsections, we aim to answer the following questions: (1) What deep transition model architecture is conducive to learning a DeepMDP on Atari? (2) How does the learning of a DeepMDP affect the overall performance of C51 on Atari 2600 games? (2) How do the DeepMDP objectives compare with similar representation-learning approaches?

8.3. Transition Model Architecture

We compare the performance achieved by using different architectures for the DeepMDP transition model (see Figure 7). We experiment with a single fully-connected layer, two fully-connected layers, and a single convolutional layer (see Appendix C for more details). We find that using a convolutional transition model leads to the best DeepMDP performance, and we use this transition model architecture for the rest of the experiments in this paper. Note how the performance of the agent is highly dependent on the architecture. We hypothesize that the inductive bias provided via the model has a large effect on the learned DeepMDPs. Further exploring model architectures which provide inductive biases is a promising avenue to develop better auxiliary tasks. Particularly, we believe that exploring attention (Vaswani et al., 2017; Bahdanau et al., 2014) and relational inductive biases (Watters et al., 2017; Battaglia et al., 2016) could be useful in visual domains like Atari2600.
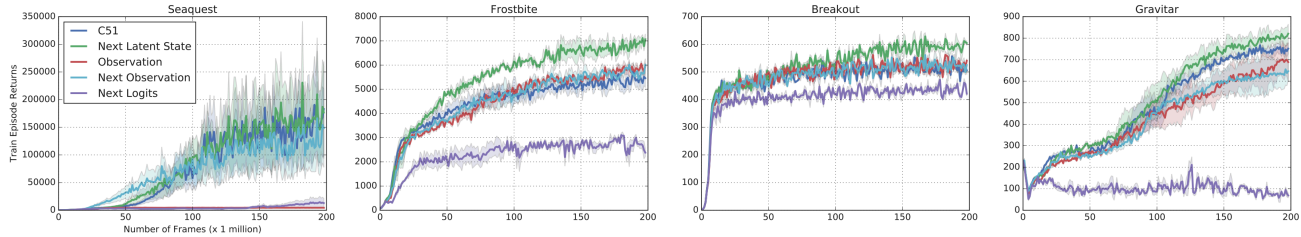
Figure 8. Using various auxiliary tasks in the Arcade Learning Environment. We compare predicting the next state's representation (Next Latent State, recommended by theoretical bounds on DeepMDPs) with reconstructing the current observation (Observation), predicting the next observation (Next Observation), and predicting the next C51 logits (Next Logits). Training curves for a baseline C51 agent are also shown.

8.4. DeepMDPs as an Auxiliary Task

We show that when using the best performing DeepMDP architecture described in Appendix *C*.2, we obtain nearly consistent performance improvements over C51 on the suite of 60 Atari 2600 games (see Figure 6).

8.5. Comparison to Alternative Objectives

We empirically compare the effect of the DeepMDP auxilliary objectives on the performance of a C51 agent to a variety of alternatives. In the experiments in this section, we replace the deep transition loss suggested by the DeepMDP bounds with each of the following:

(1) *Observation Reconstruction*: We train a state decoder to reconstruct observations $s \in \mathcal{S}$ from $\bar{s}$. This framework is similar to (Ha & Schmidhuber, 2018), who learn a latent space representation of the environment with an autoencoder, and use it to train an RL agent.

(2) *Next Observation Prediction*: We train a transition model to predict next observations $s' \sim \mathcal{P}(\cdot|s, a)$ from the current state representation $\bar{s}$. This framework is similar to model-based RL algorithms which predict future observations (Xu et al., 2018).

(3) *Next Logits Prediction*: We train a transition model to predict next-state representations such that the Q-function correctly predicts the logits of (s', a'), where a' is the action associated with the max Q-value of s'. This can be understood as a distributional analogue of the Value Prediction Network, VPN, (Oh et al., 2017). Note that this auxiliary loss is used to update only the parameters of the representation encoder and the transition model, not the Q-function.

Our experiments demonstrate that the deep transition loss suggested by the DeepMDP bounds (i.e. predicting the next state's representation) outperforms all three ablations (see Figure 8). Accurately modeling Atari 2600 frames, whether through observation reconstruction or next observation pre-

diction, forces the representation to encode irrelevant information with respect to the underlying task. VPN-style losses have been shown to be helpful when using the learned predictive model for planning (Oh et al., 2017); however, we find that with a distributional RL agent, using this as an auxiliary task tends to hurt performance.

9. Discussion on Model-Based RL

We have focused on the implications of DeepMDPs for representation learning, but our results also provide a principled basis for model-based RL – in latent space or otherwise. Although DeepMDPs are latent space models, by letting ϕ be the identity function, all the provided results immediately apply to the standard model-based RL setting, where the model predicts states instead of latent states. In fact, our results serve as a theoretical justification for common practices already found in the model-based deep RL literature. For example, Chua et al. (2018); Doerr et al. (2018); Hafner et al. (2018); Buesing et al. (2018); Feinberg et al. (2018); Buckman et al. (2018) train models to predict a reward and a distribution over next states, minimizing the negative log-probability of the true next state. The negative log-probability of the next state can be viewed as a one-sample estimate of the KL between the model's state distribution and the next state distribution. Due to Pinsker's inequality (which bounds the TV with the KL), and the suitability of TV as a metric (Section 6), this procedure can be interpreted as training a DeepMDP. Thus, the learned model will obey our local value difference bounds (Lemma 8) and suboptimality bounds (Theorem 6), which provide theoretical guarantees for the model.

Further, the suitability of Norm-MMD metrics for learning models presents a promising new research avenue for model-based RL: to break away from the KL and explore the vast family of Norm Maximum Mean Discrepancy metrics.

10. Conclusions

We introduce the concept of a DeepMDP: a parameterized latent space model trained via the minimization of tractable losses. Theoretical analysis provides guarantees on the quality of the value functions of the learned model when the latent transition loss is any member of the large family of Norm Maximum Mean Discrepancy metrics. When the Wasserstein metric is used, a novel connection to bisimulation metrics guarantees the set of parametrizable policies is highly expressive. Further, it's guaranteed that two states with different values for any of those policies will never be collapsed under the representation. Together, these findings suggest that learning a DeepMDP with the Wasserstein metric is a theoretically sound approach to representation learning. Our results are corroborated by strong performance on large-scale Atari 2600 experiments, demonstrating that minimizing the DeepMDP losses can be a beneficial auxiliary task in model-free RL.

Using the transition and reward models of the DeepMDP for model-based RL (e.g. planning, exploration) is a promising future research direction. Additionally, extending Deep-MDPs to accommodate different action spaces or time scales from the original MDPs could be a promising path towards learning hierarchical models of the environment.

Acknowledgements

Changes From ICML 2019 Proceedings

This document represents an updated version of our work relative to the version published in ICML 2019. The major addition was the inclusion of the generalization to Norm-MMD metrics and associated math in Section 6. Lemma 1 also underwent minor changes to its statements and proofs. Additionally, some sections were partially rewritten, especially the discussion on bisimulation (Section 5), which was significantly expanded.

References

Abel, D., Hershkowitz, D. E., and Littman, M. L. Near optimal behavior via approximate state abstraction. *arXiv preprint arXiv:1701.04113*, 2017.

Arjovsky, M., Chintala, S., and Bottou, L. Wasserstein generative adversarial networks. In *ICML*, 2017.

Asadi, K., Misra, D., and Littman, M. L. Lipschitz continuity in model-based reinforcement learning. *arXiv preprint arXiv:1804.07193*, 2018.

Bahdanau, D., Cho, K., and Bengio, Y. Neural machine translation by jointly learning to align and translate. *arXiv preprint arXiv:1409.0473*, 2014.

Battaglia, P. W., Pascanu, R., Lai, M., Rezende, D. J., and Kavukcuoglu, K. Interaction networks for learning about objects, relations and physics. In *NIPS*, 2016.

Bellemare, M. G., Naddaf, Y., Veness, J., and Bowling, M. The Arcade Learning Environment: An evaluation platform for general agents. *Journal of Artificial Intelligence Research*, 47:253–279, June 2013.

Bellemare, M. G., Dabney, W., and Munos, R. A distributional perspective on reinforcement learning. In *Proceedings of the International Conference on Machine Learning*, 2017a.

Bellemare, M. G., Danihelka, I., Dabney, W., Mohamed, S., Lakshminarayanan, B., Hoyer, S., and Munos, R. The cramer distance as a solution to biased wasserstein gradients. *arXiv preprint arXiv:1705.10743*, 2017b.

Bellemare, M. G., Dabney, W., Dadashi, R., Taiga, A. A., Castro, P. S., Roux, N. L., Schuurmans, D., Lattimore, T., and Lyle, C. A geometric perspective on optimal representations for reinforcement learning. *CoRR*, abs/1901.11530, 2019.

Bikowski, M., Sutherland, D. J., Arbel, M., and Gretton, A. Demystifying MMD GANs. In *International Conference on Learning Representations*, 2018. URL https://openreview.net/forum?id=r1lUOzWCW.

Borwein, J. and Lewis, A. S. *Convex Analysis and Nonlinear Optimization*. Springer, 2005.

Buckman, J., Hafner, D., Tucker, G., Brevdo, E., and Lee, H. Sample-efficient reinforcement learning with stochastic ensemble value expansion. In *NeurIPS*, 2018.

Buesing, L., Weber, T., Racaniere, S., Eslami, S., Rezende, D., Reichert, D. P., Viola, F., Besse, F., Gregor, K., Hassabis, D., et al. Learning and querying fast generative models for reinforcement learning. *arXiv preprint arXiv:1802.03006*, 2018.

Castro, P. and Precup, D. Using bisimulation for policy transfer in mdps. *Proceeedings of the 9th International Conference on Autonomous Agents and Multiagent Systems (AAMAS-2010)*, 2010.

Castro, P. S., Moitra, S., Gelada, C., Kumar, S., and Bellemare, M. G. Dopamine: A research framework for deep reinforcement learning. *arXiv*, 2018.

Chua, K., Calandra, R., McAllister, R., and Levine, S. Deep reinforcement learning in a handful of trials using probabilistic dynamics models. In *Advances in Neural Information Processing Systems*, pp. 4754–4765, 2018.

Chung, W., Nath, S., Joseph, A. G., and White, M. Two-timescale networks for nonlinear value function approximation. In *International Conference on Learning Representations*, 2019.

Comanici, G. and Precup, D. Basis function discovery using spectral clustering and bisimulation metrics. In *AAMAS*, 2011.

Dabney, W., Ostrovski, G., Silver, D., and Munos, R. Implicit quantile networks for distributional reinforcement learning. In *ICML*, 2018a.

Dabney, W., Rowland, M., Bellemare, M. G., and Munos, R. Distributional reinforcement learning with quantile regression. In *AAAI*, 2018b.

Dadashi, R., Taiga, A. A., Roux, N. L., Schuurmans, D., and Bellemare, M. G. The value function polytope in reinforcement learning. *CoRR*, abs/1901.11524, 2019.

Doerr, A., Daniel, C., Schiegg, M., Nguyen-Tuong, D., Schaal, S., Toussaint, M., and Trimpe, S. Probabilistic recurrent state-space models. *arXiv preprint arXiv:1801.10395*, 2018.

Fedus, W., Gelada, C., Bengio, Y., Bellemare, M. G., and Larochelle, H. Hyperbolic discounting and learning over multiple horizons. *ArXiv*, abs/1902.06865, 2019.

Feinberg, V., Wan, A., Stoica, I., Jordan, M. I., Gonzalez, J. E., and Levine, S. Model-based value estimation for efficient model-free reinforcement learning. *arXiv preprint arXiv:1803.00101*, 2018.

Ferns, N., Panangaden, P., and Precup, D. Metrics for finite markov decision processes. *Proceedings of the 20th Conference on Uncertainty in Artificial Intelligence*, UAI'04:162–169, 2004.

Ferns, N., Panangaden, P., and Precup, D. Bisimulation metrics for continuous markov decision processes. *SIAM Journal on Computing*, 40(6):1662–1714, 2011.

Francois-Lavet, V., Bengio, Y., Precup, D., and Pineau, J. Combined reinforcement learning via abstract representations. *arXiv preprint arXiv:1809.04506*, 2018.

Gelada, C. and Bellemare, M. G. Off-policy deep reinforcement learning by bootstrapping the covariate shift. *CoRR*, abs/1901.09455, 2019.

Givan, R., Dean, T., and Greig, M. Equivalence notions and model minimization in markov decision processes. *Artificial Intelligence*, 147(1-2):163–223, 2003.

Gouk, H., Frank, E., Pfahringer, B., and Cree, M. J. Regularisation of neural networks by enforcing lipschitz continuity. *CoRR*, abs/1804.04368, 2018.

Gretton, A., Borgwardt, K. M., Rasch, M. J., Schölkopf, B., and Smola, A. J. A kernel two-sample test. *Journal of Machine Learning Research*, 13:723–773, 2012.

Gulrajani, I., Ahmed, F., Arjovsky, M., Dumoulin, V., and Courville, A. C. Improved training of wasserstein gans. In *NIPS*, 2017a.

Gulrajani, I., Ahmed, F., Arjovsky, M., Dumoulin, V., and Courville, A. C. Improved training of wasserstein gans. In *Advances in Neural Information Processing Systems*, pp. 5767–5777, 2017b.

Ha, D. and Schmidhuber, J. Recurrent world models facilitate policy evolution. In *Advances in Neural Information Processing Systems*, pp. 2455–2467, 2018.

Hafner, D., Lillicrap, T., Fischer, I., Villegas, R., Ha, D., Lee, H., and Davidson, J. Learning latent dynamics for planning from pixels. *arXiv preprint arXiv:1811.04551*, 2018.

Hinderer, K. Lipschitz continuity of value functions in markovian decision processes. *Math. Meth. of OR*, 62:3–22, 2005.

Jaderberg, M., Mnih, V., Czarnecki, W. M., Schaul, T., Leibo, J. Z., Silver, D., and Kavukcuoglu, K. Reinforcement learning with unsupervised auxiliary tasks. *arXiv preprint arXiv:1611.05397*, 2016.

Jiang, N., Kulesza, A., and Singh, S. Abstraction selection in model-based reinforcement learning. In *International Conference on Machine Learning*, pp. 179–188, 2015.

Kaiser, L., Babaeizadeh, M., Milos, P., Osinski, B., Campbell, R. H., Czechowski, K., Erhan, D., Finn, C., Kozakowski, P., Levine, S., Sepassi, R., Tucker, G., and Michalewski, H. Model-based reinforcement learning for atari. *CoRR*, abs/1903.00374, 2019.

Li, L., Walsh, T. J., and Littman, M. L. Towards a unified theory of state abstraction for mdps. In *ISAIM*, 2006.

Lyle, C., Castro, P. S., and Bellemare, M. G. A comparative analysis of expected and distributional reinforcement learning. *CoRR*, abs/1901.11084, 2019.

Mahadevan, S. and Maggioni, M. Proto-value functions: A laplacian framework for learning representation and control in markov decision processes. *Journal of Machine Learning Research*, 8:2169–2231, 2007.

Mirowski, P. W., Pascanu, R., Viola, F., Soyer, H., Ballard, A. J., Banino, A., Denil, M., Goroshin, R., Sifre, L., Kavukcuoglu, K., Kumaran, D., and Hadsell, R. Learning to navigate in complex environments. *CoRR*, abs/1611.03673, 2017.

Mnih, V., Kavukcuoglu, K., Silver, D., Rusu, A. A., Veness, J., Bellemare, M. G., Graves, A., Riedmiller, M. A., Fidjeland, A., Ostrovski, G., Petersen, S., Beattie, C., Sadik, A., Antonoglou, I., King, H., Kumaran, D., Wierstra, D., Legg, S., and Hassabis, D. Human-level control through deep reinforcement learning. *Nature*, 518:529–533, 2015.

Mueller, A. Integral probability metrics and their generating classes of functions. 1997.

Müller, A. Integral probability metrics and their generating classes of functions. *Advances in Applied Probability*, 29 (2):429–443, 1997.

Oh, J., Singh, S., and Lee, H. Value prediction network. In *Advances in Neural Information Processing Systems*, pp. 6118–6128, 2017.

Parr, R., Li, L., Taylor, G., Painter-Wakefield, C., and Littman, M. L. An analysis of linear models, linear value-function approximation, and feature selection for reinforcement learning. In *ICML*, 2008.

Pirotta, M., Restelli, M., and Bascetta, L. Policy gradient in lipschitz markov decision processes. *Machine Learning*, 100(2-3):255–283, 2015.

Puterman, M. L. Markov decision processes: Discrete stochastic dynamic programming. 1994.

Ruan, S. S., Comanici, G., Panangaden, P., and Precup, D. Representation discovery for mdps using bisimulation metrics. In *AAAI*, 2015.

Sejdinovic, D., Sriperumbudur, B. K., Gretton, A., and Fukumizu, K. Equivalence of distance-based and rkhs-based statistics in hypothesis testing. *CoRR*, abs/1207.6076, 2013.

Silver, D., van Hasselt, H. P., Hessel, M., Schaul, T., Guez, A., Harley, T., Dulac-Arnold, G., Reichert, D. P., Rabinowitz, N. C., Barreto, A., and Degris, T. The predictron: End-to-end learning and planning. In *ICML*, 2017.

Singh, S. P., Jaakkola, T., and Jordan, M. I. Reinforcement learning with soft state aggregation. In *Advances in neural information processing systems*, pp. 361–368, 1995.

Székely, G. J. and Rizzo, M. L. Testing for equal distributions in high dimension. 2004.

van den Oord, A., Li, Y., and Vinyals, O. Representation learning with contrastive predictive coding. *CoRR*, abs/1807.03748, 2018.

Vaswani, A., Shazeer, N., Parmar, N., Uszkoreit, J., Jones, L., Gomez, A. N., Kaiser, L., and Polosukhin, I. Attention is all you need. In *NIPS*, 2017.

Villani, C. *Optimal Transport: Old and New*. Springer Science & Business Media, 2008, 2008.

Watters, N., Tacchetti, A., Weber, T., Pascanu, R., Battaglia, P. W., and Zoran, D. Visual interaction networks. *CoRR*, abs/1706.01433, 2017.

Xu, H., Li, Y., Tian, Y., Darrell, T., and Ma, T. Algorithmic framework for model-based reinforcement learning with theoretical guarantees. *arXiv preprint arXiv:1807.03858*, 2018.

Zhang, M., Vikram, S., Smith, L., Abbeel, P., Johnson, M. J., and Levine, S. Solar: Deep structured latent representations for model-based reinforcement learning. *arXiv preprint arXiv:1808.09105*, 2018.

Appendix

A. Proofs

A.1. Lipschitz MDP

Lemma 1. *Let $\overline{\mathcal{M}}$ be $(K_{\bar{\mathcal{R}}}, K_{\bar{\mathcal{P}}})$-Lipschitz. Then,*

1. *The optimal policy $\bar{\pi}^*$ is $\frac{K_{\bar{\mathcal{R}}}}{1-\gamma K_{\bar{\mathcal{P}}}}$-Lipschitz-valued.*

2. *All policies with $K_{\bar{\mathcal{P}}_{\bar{\pi}}} \leqslant \frac{1}{\gamma}$ are $\frac{K_{\bar{\mathcal{R}}_{\bar{\pi}}}}{1-\gamma K_{\bar{\mathcal{P}}_{\bar{\pi}}}}$-Lipschitz-valued.*

3. *All constant policies (i.e. $\bar{\pi}(a|\bar{s}_1) = \bar{\pi}(a|\bar{s}_2), \forall a \in \mathcal{A}, \bar{s}_1, \bar{s}_2 \in \bar{\mathcal{S}}$) are $\frac{K_{\bar{\mathcal{R}}}}{1-\gamma K_{\bar{\mathcal{P}}}}$-Lipschitz-valued.*

Proof. Start by proving **1**. By induction we will show that a sequence of Q values $\bar{Q}_n$ converging to $\bar{Q}^*$ are all Lipschitz, and that as $n \to \infty$, their Lipschitz norm goes to $\frac{K_{\bar{\mathcal{R}}}}{1-\gamma K_{\bar{\mathcal{P}}}}$. Let $\bar{Q}_0(\bar{s}, a) = 0, \forall \bar{s} \in \bar{\mathcal{S}}, a \in \mathcal{A}$ be the base case. Define $\bar{Q}_{n+1}(\bar{s}, a) = \bar{\mathcal{R}}(\bar{s}, a) + \gamma \mathbb{E}_{\bar{s}' \sim \bar{\mathcal{P}}(\cdot|\bar{s}, a)} \left[\max_{a'} \bar{Q}_n(\bar{s}', a') \right]$. It is a well known result that the sequence $\bar{Q}_n$ converges to $\bar{Q}^*$. Now let $K_{\bar{Q}, n} = \sup_{a \in \mathcal{A}, \bar{s}_1 \neq \bar{s}_2 \in \bar{\mathcal{S}}} \frac{|\bar{Q}_n(\bar{s}_1, a) - \bar{Q}_n(\bar{s}_2, a)|}{d_{\bar{\mathcal{S}}}(\bar{s}_1, \bar{s}_2)}$ be the Lipschitz norm of $\bar{Q}_n$. Clearly $K_{\bar{Q}, 0} = 0$. Then,

$$
\begin{aligned}
K_{\bar{Q}, n+1} &= \sup_{a \in \mathcal{A}, \bar{s}_1 \neq \bar{s}_2 \in \bar{\mathcal{S}}} \frac{|\bar{Q}_{n+1}(\bar{s}_1, a) - \bar{Q}_{n+1}(\bar{s}_2, a)|}{d_{\bar{\mathcal{S}}}(\bar{s}_1, \bar{s}_2)} \\
&\leqslant \sup_{a \in \mathcal{A}, \bar{s}_1 \neq \bar{s}_2 \in \bar{\mathcal{S}}} \frac{|\bar{\mathcal{R}}(\bar{s}_1, a) - \bar{\mathcal{R}}(\bar{s}_2, a)|}{d_{\bar{\mathcal{S}}}(\bar{s}_1, \bar{s}_2)} + \gamma \sup_{a \in \mathcal{A}, \bar{s}_1 \neq \bar{s}_2 \in \bar{\mathcal{S}}} \frac{| \mathbb{E}_{\bar{s}_1' \sim \bar{\mathcal{P}}(\cdot|\bar{s}_1, a)} \bar{Q}_n(\bar{s}_1', a) - \mathbb{E}_{\bar{s}_2' \sim \bar{\mathcal{P}}(\cdot|\bar{s}_2, a)} \bar{Q}_n(\bar{s}_2', a)|}{d_{\bar{\mathcal{S}}}(\bar{s}_1, \bar{s}_2)} \\
&= K_{\bar{\mathcal{R}}} + \gamma \sup_{a \in \mathcal{A}, \bar{s}_1 \neq \bar{s}_2 \in \bar{\mathcal{S}}} \frac{| \mathbb{E}_{\bar{s}_1' \sim \bar{\mathcal{P}}(\cdot|\bar{s}_1, a)} \bar{Q}_n(\bar{s}_1', a) - \mathbb{E}_{\bar{s}_2' \sim \bar{\mathcal{P}}(\cdot|\bar{s}_2, a)} \bar{Q}_n(\bar{s}_2', a)|}{d_{\bar{\mathcal{S}}}(\bar{s}_1, \bar{s}_2)} \\
&\leqslant K_{\bar{\mathcal{R}}} + \gamma K_{\bar{Q}, n} \sup_{a \in \mathcal{A}, \bar{s}_1 \neq \bar{s}_2 \in \bar{\mathcal{S}}} \frac{W\left(\bar{\mathcal{P}}(\cdot|\bar{s}_2, a), \bar{\mathcal{P}}(\cdot|\bar{s}_2, a)\right)}{d_{\bar{\mathcal{S}}}(\bar{s}_1, \bar{s}_2)}, \text{ (Using the fact that } \bar{Q}_n \text{ is } K_{\bar{Q}, n}\text{-Lipschitz by induction)} \\
&\leqslant K_{\bar{\mathcal{R}}} + \gamma K_{\bar{Q}, n} K_{\bar{\mathcal{P}}} \\
&\leqslant \sum_{i=0}^{n-1} (\gamma K_{\bar{\mathcal{P}}})^i K_{\bar{\mathcal{R}}} + (\gamma K_{\bar{\mathcal{P}}})^n K_{\bar{Q}, 0} = \sum_{i=0}^{n-1} (\gamma K_{\bar{\mathcal{P}}})^i K_{\bar{\mathcal{R}}}, \text{ (by expanding the recursion)}
\end{aligned}
$$

Thus, as $n \to \infty$, $K_{\bar{Q}*} \leqslant \frac{K_{\bar{\mathcal{R}}}}{1-\gamma K_{\bar{\mathcal{P}}}}$.

To prove **2** a similar argument can be used. The sequence $\bar{V}_{n+1}(\bar{s}, a) = \bar{\mathcal{R}}_{\bar{\pi}}(\bar{s}) + \gamma \mathbb{E}_{\bar{s}' \sim \bar{\mathcal{P}}(\cdot|\bar{s}, a)} \left[\bar{V}_n(\bar{s}') \right]$ converges to $\bar{Q}^{\bar{\pi}}$ and the sequence of Lipschitz norms converge to $\frac{K_{\bar{\mathcal{R}}_{\bar{\pi}}}}{1-\gamma K_{\bar{\mathcal{P}}}}$. From there it's trivial to show that $\bar{Q}^{\bar{\pi}}$ is also Lipschitz.

Finally, we prove **3**. Note that the transition function of a constant policy $\pi(a)$ has the following property:

$$
\begin{aligned}
W\left(\bar{\mathcal{P}}_{\bar{\pi}}(\cdot|\bar{s}_2), \bar{\mathcal{P}}_{\bar{\pi}}(\cdot|\bar{s}_2)\right) &= \sup_{f \in \mathcal{F}} \left| \int (\bar{\mathcal{P}}_{\bar{\pi}}(\bar{s}'|\bar{s}_2) - \bar{\mathcal{P}}_{\bar{\pi}}(\bar{s}'|\bar{s}_2)) f(\bar{s}') \, d\bar{s}' \right| \\
&\leqslant \sup_{f \in \mathcal{F}} \left| \int \sum_a \pi(a) (\bar{\mathcal{P}}(\bar{s}'|\bar{s}_2, a) - \bar{\mathcal{P}}(\bar{s}'|\bar{s}_2, a)) f(\bar{s}') \, d\bar{s}' \right| \\
&\leqslant \sum_a \pi(a) \sup_{f \in \mathcal{F}} \left| \int (\bar{\mathcal{P}}(\bar{s}'|\bar{s}_2, a) - \bar{\mathcal{P}}(\bar{s}'|\bar{s}_2, a)) f(\bar{s}') \, d\bar{s}' \right| \\
&\leqslant \sum_a \pi(a) K_{\bar{\mathcal{P}}} \\
&\leqslant K_{\bar{\mathcal{P}}}
\end{aligned}
$$

Similarly, $|\bar{\mathcal{R}}_{\bar{\pi}}(\bar{s}_1) - \bar{\mathcal{R}}_{\bar{\pi}}(\bar{s}_2)| \leqslant K_{\bar{\mathcal{R}}}$. Thus, for a constant policy π, the Lipschitz norms $K_{\bar{\mathcal{P}}_{\bar{\pi}}} \leqslant K_{\bar{\mathcal{P}}}$ and $K_{\bar{\mathcal{R}}_{\bar{\pi}}} \leqslant K_{\bar{\mathcal{R}}}$. To complete the proof we can apply result **2**. $\qquad \square$

A.2. Global DeepMDP

Lemma 2. *Let $\mathcal{M}$ and $\overline{\mathcal{M}}$ be an MDP and DeepMDP respectively, with an embedding function ϕ and global loss functions $L_{\mathcal{R}}^{\infty}$ and $L_{\mathcal{P}}^{\infty}$. For any $K_{\bar{V}}$-Lipschitz-valued policy $\bar{\pi} \in \bar{\Pi}$ the value difference can be bounded by*

$$\left| Q^{\bar{\pi}}(s,a) - \bar{Q}^{\bar{\pi}}(\phi(s),a) \right| \leqslant \frac{L_{\mathcal{R}}^{\infty} + \gamma K_{\bar{V}} L_{\mathcal{P}}^{\infty}}{1-\gamma},$$

Proof. This is a specific case to the general Lemma 7 $\qquad\qquad\square$

Theorem 1. *Let $\mathcal{M}$ and $\overline{\mathcal{M}}$ be an MDP and DeepMDP respectively, let $d_{\bar{\mathcal{S}}}$ be a metric in $\bar{\mathcal{S}}$, ϕ be an embedding function and $L_{\mathcal{R}}^{\infty}$ and $L_{\mathcal{P}}^{\infty}$ be the global loss functions. For any $K_{\bar{V}}$-Lipschitz-valued policy $\bar{\pi} \in \bar{\Pi}$ the representation ϕ guarantees that for all $s_1, s_2 \in \mathcal{S}$ and $a \in \mathcal{A}$,*

$$\left| Q^{\bar{\pi}}(s_1,a) - Q^{\bar{\pi}}(s_2,a) \right| \leqslant K_{\bar{V}} d_{\bar{\mathcal{S}}}(\phi(s_1), \phi(s_2))$$

$$+ 2\frac{L_{\mathcal{R}}^{\infty} + \gamma K_{\bar{V}} L_{\mathcal{P}}^{\infty}}{1-\gamma}$$

Proof.

$$\left| Q^{\bar{\pi}}(s_1,a) - Q^{\bar{\pi}}(s_2,a) \right| \leqslant \left| \bar{Q}^{\bar{\pi}}(s_1,a) - \bar{Q}^{\bar{\pi}}(s_2,a) \right| + \left| Q^{\bar{\pi}}(s_1,a) - \bar{Q}^{\bar{\pi}}(s_1,a) \right| + \left| Q^{\bar{\pi}}(s_2,a) - \bar{Q}^{\bar{\pi}}(s_2,a) \right|$$

$$\leqslant \left| \bar{Q}^{\bar{\pi}}(s_1,a) - \bar{Q}^{\bar{\pi}}(s_2,a) \right| + 2\frac{\left(L_{\mathcal{R}}^{\infty} + \gamma K_V L_{\mathcal{P}}^{\infty} \right)}{1-\gamma} \text{ Applying Lemma 2}$$

$$\leqslant K_V \left\| \phi(s_1) - \phi(s_2) \right\| + 2\frac{\left(L_{\mathcal{R}}^{\infty} + \gamma K_V L_{\mathcal{P}}^{\infty} \right)}{1-\gamma} \text{ Using the Lipschitz property of } \bar{Q}^{\bar{\pi}}$$

$$\square$$

Theorem 5. *Let $\mathcal{M}$ and $\overline{\mathcal{M}}$ be an MDP and a $(K_{\bar{\mathcal{R}}}, K_{\bar{\mathcal{P}}})$-Lipschitz DeepMDP respectively, with an embedding function ϕ and global loss functions $L_{\mathcal{R}}^{\infty}$ and $L_{\mathcal{P}}^{\infty}$. For all $s \in \mathcal{S}$, the suboptimality of the optimal policy $\bar{\pi}^*$ of $\overline{\mathcal{M}}$ evaluated on $\mathcal{M}$ can be bounded by:*

$$V^*(s) - V^{\bar{\pi}^*}(s) \leqslant 2\frac{L_{\mathcal{R}}^{\infty}}{1-\gamma} + 2\gamma\frac{K_{\bar{\mathcal{R}}} L_{\mathcal{P}}^{\infty}}{(1-\gamma)(1-\gamma K_{\bar{\mathcal{P}}})}$$

Proof. This is just a case of the general Theorem 6 combined with the result that the optimal policy of a $(K_{\bar{\mathcal{R}}}, K_{\bar{\mathcal{P}}})$-Lipschitz DeepMDP is $\frac{K_{\bar{\mathcal{R}}}}{1-\gamma K_{\bar{\mathcal{P}}}}$-Lipschitz-valued. $\qquad\qquad\square$

A.3. Local DeepMDP

Lemma 3. *Let $\mathcal{M}$ and $\overline{\mathcal{M}}$ be an MDP and DeepMDP respectively, with an embedding function ϕ. For any $K_{\bar{V}}$-Lipschitz-valued policy $\bar{\pi} \in \bar{\Pi}$, the expected value function difference can be bounded using the local loss functions $L_{\mathcal{R}}^{\xi_{\bar{\pi}}}$ and $L_{\mathcal{P}}^{\xi_{\bar{\pi}}}$ measured under $\xi_{\bar{\pi}}$, the stationary state action distribution of $\bar{\pi}$.*

$$\mathop{\mathbb{E}}_{s,a \sim \xi_{\bar{\pi}}} \left| Q^{\bar{\pi}}(s,a) - \bar{Q}^{\bar{\pi}}(\phi(s),a) \right| \qquad\qquad \leqslant \qquad\qquad \frac{L_{\mathcal{R}}^{\xi_{\bar{\pi}}} + \gamma K_{\bar{V}} L_{\mathcal{P}}^{\xi_{\bar{\pi}}}}{1-\gamma},$$

Proof. This Lemma is just an example of the general Lemma 8 $\qquad\qquad\square$

Theorem 2. *Let $\mathcal{M}$ and $\overline{\mathcal{M}}$ be an MDP and DeepMDP respectively, let $d_{\bar{\mathcal{S}}}$ be the metric in $\bar{\mathcal{S}}$ and ϕ be the embedding function. Let $\bar{\pi} \in \bar{\Pi}$ be any $K_{\bar{V}}$-Lipschitz-valued policy with stationary distribution $\xi_{\bar{\pi}}$, and let $L_{\mathcal{R}}^{\xi_{\bar{\pi}}}$ and $L_{\mathcal{P}}^{\xi_{\bar{\pi}}}$ be the local loss functions. For any two states $s_1, s_2 \in \mathcal{S}$, the representation ϕ is such that,*

$$\left| V^{\bar{\pi}}(s_1) - V^{\bar{\pi}}(s_2) \right| \leqslant K_{\bar{V}} d_{\bar{\mathcal{S}}}(\phi(s_1), \phi(s_2))$$

$$+ \frac{L_{\mathcal{R}}^{\xi_{\bar{\pi}}} + \gamma K_{\bar{V}} L_{\mathcal{P}}^{\xi_{\bar{\pi}}}}{1-\gamma} \left(\frac{1}{d_{\bar{\pi}}(s_1)} + \frac{1}{d_{\bar{\pi}}(s_2)} \right)$$

Proof. $\mathbb{E}_{s \sim \xi_{\bar{\pi}}}$

Using the fact that $\left| V^{\bar{\pi}}(s) - \bar{V}^{\bar{\pi}}(s) \right| \leqslant d_{\bar{\pi}}^{-1}(s) \mathbb{E}_{s \sim \xi_{\bar{\pi}}} \left| V^{\bar{\pi}}(s) - \bar{V}^{\bar{\pi}}(s) \right|,$

$$
\begin{aligned}
\left| V^{\bar{\pi}}(s_1) - V^{\bar{\pi}}(s_2) \right| &\leqslant \left| \bar{V}^{\bar{\pi}}(s_1) - \bar{V}^{\bar{\pi}}(s_2) \right| + d_{\bar{\pi}}^{-1}(s_1) \mathop{\mathbb{E}}_{s \sim \xi_{\bar{\pi}}} \left| V^{\bar{\pi}}(s_1) - \bar{V}^{\bar{\pi}}(s_1) \right| + d_{\bar{\pi}}^{-1}(s_2) \mathop{\mathbb{E}}_{s \sim \xi_{\bar{\pi}}} \left| V^{\bar{\pi}}(s_2) - \bar{V}^{\bar{\pi}}(s_2) \right| \\
&\leqslant \left| \bar{V}^{\bar{\pi}}(s_1) - \bar{V}^{\bar{\pi}}(s_2) \right| + \frac{L_{\bar{\mathcal{R}}}^{\xi_{\bar{\pi}}} + \gamma K_V L_{\bar{\mathcal{P}}}^{\xi_{\bar{\pi}}}}{1 - \gamma} \left(d_{\bar{\pi}}^{-1}(s_1) + d_{\bar{\pi}}^{-1}(s_2) \right), \text{ Applying Lemma 3} \\
&\leqslant K_{\bar{V}} d_{\bar{\mathcal{S}}}(\phi(s_1), \phi(s_2)) + \frac{L_{\bar{\mathcal{R}}}^{\xi_{\bar{\pi}}} + \gamma K_V L_{\bar{\mathcal{P}}}^{\xi_{\bar{\pi}}}}{1 - \gamma} \left(d_{\bar{\pi}}^{-1}(s_1) + d_{\bar{\pi}}^{-1}(s_2) \right)
\end{aligned}
$$

$\square$

A.4. Connection to Bisimulation

Lemma 4. *Let $\bar{\mathcal{M}}$ be a $K_{\mathcal{R}}$-$K_{\mathcal{P}}$-Lipschitz DeepMDP with a metric in the state space $d_{\bar{\mathcal{S}}}$. Then the bisimulation metric $\tilde{d}$ is Lipschitz s.t. $\forall \bar{s}_1, \bar{s}_2 \in \bar{\mathcal{S}}$,*

$$
\tilde{d}(\bar{s}_1, \bar{s}_2) \leqslant \frac{(1 - \gamma) K_{\bar{\mathcal{R}}}}{1 - \gamma K_{\bar{\mathcal{P}}}} d_{\bar{\mathcal{S}}}(\bar{s}_1, \bar{s}_2). \tag{9}
$$

Proof. We first derive a property of the Wasserstein. Let d and p be pseudometrics in χ s.t. $d(x, y) \leqslant K p(x, y)$ for all $x, y \in \chi$, and let P and Q be two distributions in χ. Then $W_d(P, Q) \leqslant K W_p(P, Q)$. To prove it, first note that define the sets of C-Lipschitz functions for both metrics:

$$
\begin{aligned}
\mathcal{F}_{d,C} &= \left\{ f : \forall x \neq y \in \chi, |f(x) - f(y)| \leqslant C d(x, y) \right\}, \\
\mathcal{F}_{p,C} &= \left\{ f : \forall x \neq y \in \chi, |f(x) - f(y)| \leqslant C p(x, y) \right\}.
\end{aligned}
$$

Then it becomes clear that $\mathcal{F}_{d,1} \subseteq \mathcal{F}_{p,K}$. We can now prove the property:

$$
\begin{aligned}
W_d(P, Q) &= \sup_{f \in \mathcal{F}_{d,1}} \left| \mathop{\mathbb{E}}_{x \sim P} f(x) - \mathop{\mathbb{E}}_{y \sim Q} f(y) \right| \\
&\leqslant \sup_{f \in \mathcal{F}_{p,K}} \left| \mathop{\mathbb{E}}_{x \sim P} f(x) - \mathop{\mathbb{E}}_{y \sim Q} f(y) \right| \\
&= \sup_{f \in \mathcal{F}_{p,1}} \left| \mathop{\mathbb{E}}_{x \sim P} K f(x) - \mathop{\mathbb{E}}_{y \sim Q} K f(y) \right| \\
&= K \sup_{f \in \mathcal{F}_{p,1}} \left| \mathop{\mathbb{E}}_{x \sim P} f(x) - \mathop{\mathbb{E}}_{y \sim Q} f(y) \right| \\
&= K W_p(P, Q)
\end{aligned}
$$

We prove the Lemma by induction. We show that a sequence of pseudometrics values d_n converging to $\tilde{d}$ are all Lipschitz, and that as $n \to \infty$, their Lipschitz norm goes to $\frac{(1-\gamma)K_{\bar{\mathcal{R}}}}{1-\gamma K_{\bar{\mathcal{P}}}}$. Let $d_0(s_1, s_2) = 0, \forall s_1, s_2 \in \mathcal{S}$ be the base case. Define $d_{n+1}(s_1, s_2) = F_d(s_1, s_2)$ as defined in Definition 5. Ferns et al. (2011) shows that F is a contraction, and that d_n converges

to $\widetilde{d}$ as $n \to \infty$. Now let $K_{d,n} = \sup\limits_{s_1 \neq s_2 \in \mathcal{S}} \frac{d_n(s_1, s_2)}{d_{\mathcal{S}}(s_1, s_2)}$ be the Lipschitz norm of d_n. Also see that $K_{d,0} = 0$. Then,

$$
\begin{aligned}
K_{d,n+1} &= \sup_{s_1 \neq s_2 \in \mathcal{S}} \frac{d_{n+1}(s_1, s_2)}{d_{\mathcal{S}}(s_1, s_2)} \\
&= \sup_{s_1 \neq s_2 \in \mathcal{S}} \frac{F_{d_n}(s_1, s_2)}{d_{\mathcal{S}}(s_1, s_2)} \\
&\leqslant (1-\gamma) \sup_{a \in \mathcal{A}, s_1 \neq s_2 \in \mathcal{S}} \frac{|\mathcal{R}(s_1, a) - \mathcal{R}(s_2, a)|}{d_{\mathcal{S}}(s_1, s_2)} + \gamma \sup_{a \in \mathcal{A}, s_1 \neq s_2 \in \mathcal{S}} \frac{W_{d_n}\left(\mathcal{P}(\cdot|s_2, a), \mathcal{P}(\cdot|s_2, a)\right)}{d_{\mathcal{S}}(s_1, s_2)} \\
&= (1-\gamma) K_{\mathcal{R}} + \gamma \sup_{a \in \mathcal{A}, s_1 \neq s_2 \in \mathcal{S}} \frac{W_{d_n}\left(\mathcal{P}(\cdot|s_2, a), \mathcal{P}(\cdot|s_2, a)\right)}{d_{\mathcal{S}}(s_1, s_2)} \\
&\leqslant (1-\gamma) K_{\mathcal{R}} + \gamma K_{d,n} \sup_{a \in \mathcal{A}, s_1 \neq s_2 \in \mathcal{S}} \frac{W_{d_{\mathcal{S}}}\left(\mathcal{P}(\cdot|s_2, a), \mathcal{P}(\cdot|s_2, a)\right)}{d_{\mathcal{S}}(s_1, s_2)}, \quad \text{(Using the property derived above.)} \\
&\leqslant (1-\gamma) K_{\mathcal{R}} + \gamma K_{d,n} K_{\mathcal{P}} \\
&\leqslant (1-\gamma) \sum_{i=0}^{n-1} (\gamma K_{\mathcal{P}})^i K_{\mathcal{R}}, \quad \text{(by expanding the recursion)}
\end{aligned}
$$

Thus, even as $n \to \infty$, $K_{d,n} \leqslant \frac{(1-\gamma) K_{\overline{\mathcal{R}}}}{1 - \gamma K_{\overline{\mathcal{P}}}}$. $\qquad\qquad\square$

Lemma 5. *Let $\mathcal{M}$ be an MDP and $\overline{\mathcal{M}}$ be a $K_{\overline{\mathcal{R}}}$-$K_{\overline{\mathcal{P}}}$-Lipschitz MDP with an embedding function $\phi: \mathcal{S} \to \overline{\mathcal{S}}$ and global DeepMDP losses $L_{\overline{\mathcal{P}}}^{\infty}$ and $L_{\overline{\mathcal{R}}}^{\infty}$.. We can extend the bisimulation metric to also measure a distance between $s \in \mathcal{S}$ and $\overline{s} \in \overline{\mathcal{S}}$ by considering an joined MDP constructed by joining $\mathcal{M}$ and $\overline{\mathcal{M}}$. When an action is taken, each state will transition according to the transition function of its corresponding MDP. Then the bisimulation metric between a state $s \in \mathcal{S}$ and it's embedded counterpart $\phi(s)$ is bounded by:*

$$
\widetilde{d}(s, \phi(s)) \leqslant L_{\overline{\mathcal{R}}}^{\infty} + \gamma L_{\overline{\mathcal{P}}}^{\infty} \frac{K_{\overline{\mathcal{R}}}}{1 - \gamma K_{\overline{\mathcal{P}}}}
$$

Proof. First, note that

$$
\begin{aligned}
W_{\widetilde{d}}(\phi \mathcal{P}(\cdot|s, a), \overline{\mathcal{P}}(\cdot|\phi(s), a)) &= \sup_{f \in \mathbb{F}_{\widetilde{d}}} \mathbb{E}_{\overline{s}_1' \sim \phi \mathcal{P}(\cdot|s,a)}[f(\overline{s}_1')] - \mathbb{E}_{\overline{s}_2' \sim \overline{\mathcal{P}}(\cdot|\phi(s),a)}[f(\overline{s}_2')] \\
&\leqslant \frac{(1-\gamma) K_{\mathcal{R}}}{1 - \gamma K_{\mathcal{P}}} \sup_{f \in \mathbb{F}_1} \mathbb{E}_{\overline{s}_1' \sim \phi \mathcal{P}(\cdot|s,a)}[f(\overline{s}_1')] - \mathbb{E}_{\overline{s}_2' \sim \overline{\mathcal{P}}(\cdot|\phi(s),a)}[f(\overline{s}_2')] \quad \text{(Using Theorem 4)} \\
&= \frac{(1-\gamma) K_{\mathcal{R}}}{1 - \gamma K_{\mathcal{P}}} W_{\ell_2}(\mathcal{P}(\cdot|s, a), \overline{\mathcal{P}}(\cdot|\phi(s), a)) \\
&\leqslant \frac{(1-\gamma) K_{\mathcal{R}}}{1 - \gamma K_{\mathcal{P}}} L_{\overline{\mathcal{P}}}^{\infty}
\end{aligned}
$$

Using the triangle inequality of pseudometrics and the previous derivation:

$$
\begin{aligned}
\sup_s \widetilde{d}(s, \phi(s)) &= \max_{a \in \mathcal{A}} \left((1-\gamma) |\mathcal{R}(s, a) - \overline{\mathcal{R}}(\phi(s), a)| + \gamma W_{\widetilde{d}}(\mathcal{P}(\cdot|s, a), \overline{\mathcal{P}}(\cdot|\phi(s), a)) \right) \\
&\leqslant (1-\gamma) L_{\overline{\mathcal{R}}}^{\infty} + \gamma \max_{a \in \mathcal{A}} \left(W_{\widetilde{d}}(\mathcal{P}(\cdot|s, a), \phi \mathcal{P}(\cdot|s, a)) + W_{\widetilde{d}}(\phi \mathcal{P}(\cdot|s, a), \overline{\mathcal{P}}(\cdot|\phi(s), a)) \right) \\
&\leqslant (1-\gamma) L_{\overline{\mathcal{R}}}^{\infty} + \gamma \frac{(1-\gamma) K_{\mathcal{R}}}{1 - \gamma K_{\mathcal{P}}} L_{\overline{\mathcal{P}}}^{\infty} + \gamma \max_{a \in \mathcal{A}} W_{\widetilde{d}}(\mathcal{P}(\cdot|s, a), \phi \mathcal{P}(\cdot|s, a)) \\
&\leqslant (1-\gamma) L_{\overline{\mathcal{R}}}^{\infty} + \gamma \frac{(1-\gamma) K_{\mathcal{R}}}{1 - \gamma K_{\mathcal{P}}} L_{\overline{\mathcal{P}}}^{\infty} + \gamma \sup_s \widetilde{d}(s', \phi(s))
\end{aligned}
$$

Solving for the recurrence leads to the desired result. $\qquad\qquad\square$

Theorem 3. *Let $\mathcal{M}$ be an MDP and $\overline{\mathcal{M}}$ be a $K_{\overline{\mathcal{R}}}$-$K_{\overline{\mathcal{P}}}$-Lipschitz DeepMDP with metric $d_{\overline{\mathcal{S}}}$. Let ϕ be the embedding function and $L_{\overline{\mathcal{P}}}^{\infty}$ and $L_{\overline{\mathcal{R}}}^{\infty}$ be the global DeepMDP losses. The bisimulation distance in $\mathcal{M}$, $\widetilde{d} : \mathcal{S} \times \mathcal{S} \to \mathbb{R}^+$ can be upperbounded by the ℓ_2 distance in the embedding and the losses in the following way:*

$$\widetilde{d}(s_1, s_2) \leqslant \frac{(1-\gamma)K_{\mathcal{R}}}{1 - \gamma K_{\overline{\mathcal{P}}}} d_{\overline{\mathcal{S}}}(\phi(s_1), \phi(s_2))$$

$$+ 2 \left(L_{\overline{\mathcal{R}}}^{\infty} + \gamma L_{\overline{\mathcal{P}}}^{\infty} \frac{K_{\overline{\mathcal{R}}}}{1 - \gamma K_{\overline{\mathcal{P}}}} \right)$$

Proof.

$$\widetilde{d}(s_1, s_2) \leqslant \widetilde{d}(s_1, \phi(s_1)) + \widetilde{d}(s_2, \phi(s_2)) + \widetilde{d}(\phi(s_1), \phi(s_2))$$

$$\leqslant 2 \left(L_{\overline{\mathcal{R}}}^{\infty} + \gamma L_{\overline{\mathcal{P}}}^{\infty} \frac{K_{\overline{\mathcal{R}}}}{1 - \gamma K_{\overline{\mathcal{P}}}} \right) + \widetilde{d}(\phi(s_1), \phi(s_2)) \qquad \text{(Using Theorem 5)}$$

$$\leqslant 2 \left(L_{\overline{\mathcal{R}}}^{\infty} + \gamma L_{\overline{\mathcal{P}}}^{\infty} \frac{K_{\overline{\mathcal{R}}}}{1 - \gamma K_{\overline{\mathcal{P}}}} \right) + \frac{(1-\gamma)L_{\overline{\mathcal{R}}}^{\infty}}{1 - \gamma K_{\overline{\mathcal{P}}}} \|\phi(s_1) - \phi(s_2)\| \qquad \text{(Applying Theorem 4)}$$

Completing the proof. □

A.5. Quality of $\overline{\Pi}$

Lemma 6. *Let d_f and d_g be the metrics on the space χ, with the property that for some $\epsilon \geqslant 0$ it holds that $\forall x, y \in \chi, d_f(x, y) \leqslant \epsilon + d_g(x, y)$. Define the sets of 1-Lipschitz functions $\mathbb{F} = \{f : |f(x) - f(y)| \leqslant d_f(x, y), \forall x, y \in \chi\}$ and $\mathbb{G} = \{g : |g(x) - g(y)| \leqslant d_g(x, y), \forall x, y \in \chi\}$. Then for any $f \in \mathbb{F}$, there exists one $g \in \mathbb{G}$ such that for all $x \in \chi$,*

$$|f(x) - g(x)| \leqslant \frac{\epsilon}{2}$$

Proof. Define the set $\mathbb{Z} = \{z : |z(x) - z(y)| \leqslant \epsilon + d_g(x, y), \forall x, y \in \chi\}$. Then trivially, any function $f \in \mathbb{F}$ is also a member of $\mathbb{Z}$. We now show that the set $\mathbb{Z}$ can equivalently be expressed as $z(x) = g(x) + u(x)$, where $g \in \mathbb{G}$ and $u(x) \in (\frac{-\epsilon}{2}, \frac{\epsilon}{2})$, is (non Lipschitz) bounded function.

$$|z(x) - z(y)| = |g(x) + u(x) - g(y) - u(y)|$$
$$\leqslant |g(x) - g(y)| + |u(x) - u(y)|$$
$$\leqslant d_g(x, y) + \epsilon$$

Note how both inequalities are tight (there is a g and u for which the equality holds), together with the fact that the set $\mathbb{Z}$ is convex, it follows that any $z \in \mathbb{Z}$ must be expressible as $g(x) + u(x)$.

We now complete the proof. For any $z \in \mathbb{Z}$, there exist a $g \in \mathbb{G}$ s.t. $z(x) = g(x) + u(x)$. Then:

$$|z(x) - g(x)| = |u(x)| \leqslant \frac{\epsilon}{2}$$

□

Theorem 4. *Let $\mathcal{M}$ be an MDP and $\overline{\mathcal{M}}$ be a $(K_{\overline{\mathcal{R}}}, K_{\overline{\mathcal{P}}})$-Lipschitz DeepMDP, with an embedding function ϕ and global loss functions $L_{\overline{\mathcal{R}}}^{\infty}$ and $L_{\overline{\mathcal{P}}}^{\infty}$. Denote by $\widetilde{\Pi}_K$ and $\overline{\Pi}_K$ the sets of Lipschitz-bisimilar and Lipschitz-deep policies. Then for any $\widetilde{\pi} \in \widetilde{\Pi}_K$ there exists a $\overline{\pi} \in \overline{\Pi}_{CK}$ which is close to $\widetilde{\pi}$ in the sense that, for all $s \in \mathcal{S}$ and $a \in \mathcal{A}$,*

$$|\widetilde{\pi}(a|s) - \overline{\pi}(a|s)| \leqslant L_{\overline{\mathcal{R}}}^{\infty} + \gamma L_{\overline{\mathcal{P}}}^{\infty} \frac{K_{\overline{\mathcal{R}}}}{1 - \gamma K_{\overline{\mathcal{P}}}}$$

Proof. The proof is based on Lemma 6. Let $\chi = \mathcal{S}$, $d_f(x, y) = K\widetilde{d}(x, y)$, $d_g(x, y) = KC \|\phi(x) - \phi(y)\|$ and $\epsilon = 2 \left(L_{\overline{\mathcal{R}}}^{\infty} + \gamma L_{\overline{\mathcal{P}}}^{\infty} \frac{K_{\overline{\mathcal{R}}}}{1 - \gamma K_{\overline{\mathcal{P}}}} \right)$. Theorem 3 can be used to show that the condition $d_f(x, y) \leqslant \epsilon + d_g(x, y)$ holds. Then the application of Lemma 6 provides the desired result. □

A.6. Generalized Value Difference Bounds

Lemma 7. *Let $\mathcal{M}$ and $\overline{\mathcal{M}}$ be an MDP and DeepMDP respectively, with an embedding function ϕ and global loss functions $L_{\mathcal{R}}^{\infty}$ and $L_{\mathcal{P}}^{\infty}$, where $L_{\mathcal{P}}^{\infty}$ uses on a Norm-MMD $\mathcal{D}$. For any $K_{\bar{V}}$-smooth-valued policy $\bar{\pi} \in \bar{\Pi}$ as in Definition 7. The value difference can be bounded by*

$$\left| Q^{\bar{\pi}}(s,a) - \bar{Q}^{\bar{\pi}}(\phi(s),a) \right| \leqslant \frac{L_{\mathcal{R}}^{\infty} + \gamma K_{\bar{V}} L_{\mathcal{P}}^{\infty}}{1-\gamma}.$$

Proof. The proof consists of showing that the supremum $\sup_{s,a} \left| Q^{\bar{\pi}}(s,a) - \bar{Q}^{\bar{\pi}}(\phi(s),a) \right|$ is bounded by a recurrence relationship.

$$\sup_{s\in\mathcal{S},a\in\mathcal{A}} \left| Q^{\bar{\pi}}(s,a) - \bar{Q}^{\bar{\pi}}(\phi(s),a) \right| \leqslant \sup_{s\in\mathcal{S},a\in\mathcal{A}} \left| \mathcal{R}(s,a) - \bar{\mathcal{R}}(\phi(s),a) \right| + \gamma \sup_{s\in\mathcal{S},a\in\mathcal{A}} \left| \underset{s'\sim\mathcal{P}(\cdot|s,a)}{\mathbb{E}} V^{\bar{\pi}}(s') - \underset{\bar{s}'\sim\bar{\mathcal{P}}(\cdot|\phi(s),a)}{\mathbb{E}} \bar{V}^{\bar{\pi}}(\bar{s}') \right|$$

$$= L_{\mathcal{R}}^{\infty} + \gamma \sup_{s\in\mathcal{S},a\in\mathcal{A}} \left| \underset{s'\sim\mathcal{P}(\cdot|s,a)}{\mathbb{E}} [V^{\bar{\pi}}(s') - \bar{V}^{\bar{\pi}}(\phi(s'))] + \underset{\substack{\bar{s}'\sim\bar{\mathcal{P}}(\cdot|\phi(s),a) \\ s'\sim\mathcal{P}(\cdot|s,a)}}{\mathbb{E}} [\bar{V}^{\bar{\pi}}(\phi(s')) - \bar{V}^{\bar{\pi}}(\bar{s}')] \right|$$

$$\leqslant L_{\mathcal{R}}^{\infty} + \gamma \sup_{s\in\mathcal{S},a\in\mathcal{A}} \left| \underset{s'\sim\mathcal{P}(\cdot|s,a)}{\mathbb{E}} [V^{\bar{\pi}}(s') - \bar{V}^{\bar{\pi}}(\phi(s'))] \right| + \gamma \sup_{s\in\mathcal{S},a\in\mathcal{A}} \left| \underset{\substack{\bar{s}'\sim\bar{\mathcal{P}}(\cdot|\phi(s),a) \\ s'\sim\mathcal{P}(\cdot|s,a)}}{\mathbb{E}} [\bar{V}^{\bar{\pi}}(\phi(s')) - \bar{V}^{\bar{\pi}}(\bar{s}')] \right|$$

$$\leqslant L_{\mathcal{R}}^{\infty} + \gamma \sup_{s\in\mathcal{S},a\in\mathcal{A}} \left| \underset{s'\sim\mathcal{P}(\cdot|s,a)}{\mathbb{E}} [V^{\bar{\pi}}(s') - \bar{V}^{\bar{\pi}}(\phi(s'))] \right| + \gamma K_{\bar{V}} \sup_{s\in\mathcal{S},a\in\mathcal{A}} \mathcal{D}\left(\phi\mathcal{P}(\cdot|s,a), \bar{\mathcal{P}}(\cdot|\phi(s),a) \right)$$

$$= L_{\mathcal{R}}^{\infty} + \gamma \sup_{s\in\mathcal{S},a\in\mathcal{A}} \left| \underset{s'\sim\mathcal{P}(\cdot|s,a)}{\mathbb{E}} [V^{\bar{\pi}}(s') - \bar{V}^{\bar{\pi}}(\phi(s'))] \right| + \gamma K_{\bar{V}} L_{\mathcal{P}}^{\infty}$$

$$\leqslant L_{\mathcal{R}}^{\infty} + \gamma \sup_{s\in\mathcal{S},a\in\mathcal{A}} \underset{s'\sim\mathcal{P}(\cdot|s,a)}{\mathbb{E}} \left| [V^{\bar{\pi}}(s') - \bar{V}^{\bar{\pi}}(\phi(s'))] \right| + \gamma K_{\bar{V}} L_{\mathcal{P}}^{\infty} \text{ Using Jensen's inequality.}$$

$$\leqslant L_{\mathcal{R}}^{\infty} + \gamma \sup_{s\in\mathcal{S},a\in\mathcal{A}} \left| [V^{\bar{\pi}}(s) - \bar{V}^{\bar{\pi}}(\phi(s))] \right| + \gamma K_{\bar{V}} L_{\mathcal{P}}^{\infty}$$

$$\leqslant L_{\mathcal{R}}^{\infty} + \gamma \sup_{s\in\mathcal{S},a\in\mathcal{A}} \left| [Q^{\bar{\pi}}(s,a) - \bar{Q}^{\bar{\pi}}(\phi(s),a)] \right| + \gamma K_{\bar{V}} L_{\mathcal{P}}^{\infty}$$

Solving for the recurrence relation over $\sup_{s\in\mathcal{S},a\in\mathcal{A}} \left| Q^{\bar{\pi}}(s,a) - \bar{Q}^{\bar{\pi}}(\phi(s),a) \right|$ results in the desired result. $\square$

Lemma 8. *Let $\mathcal{M}$ and $\overline{\mathcal{M}}$ be an MDP and DeepMDP respectively, with an embedding function ϕ and let $\mathcal{D}$ be a Norm-MMD metric. For any $K_{\bar{V}}$-smooth-valued policy $\bar{\pi} \in \bar{\Pi}$ (as in Definition 7), let $L_{\mathcal{R}}^{\xi_{\bar{\pi}}}$ and $L_{\mathcal{P}}^{\xi_{\bar{\pi}}}$ be the local loss functions measured under $\xi_{\bar{\pi}}$, the stationary state action distribution of $\bar{\pi}$. Then the value difference can be bounded by:*

$$\underset{s,a\sim\xi_{\bar{\pi}}}{\mathbb{E}} \left| Q^{\bar{\pi}}(s,a) - \bar{Q}^{\bar{\pi}}(\phi(s),a) \right| \qquad\qquad \leqslant \qquad\qquad \frac{L_{\mathcal{R}}^{\xi_{\bar{\pi}}} + \gamma K_{\bar{V}} L_{\mathcal{P}}^{\xi_{\bar{\pi}}}}{1-\gamma},$$

Proof.

$$\mathop{\mathbb{E}}_{s,a\sim\xi_{\bar{\pi}}}\left|Q^{\bar{\pi}}(s,a)-\bar{Q}^{\bar{\pi}}(\phi(s),a)\right|\leqslant\mathop{\mathbb{E}}_{s,a\sim\xi_{\bar{\pi}}}\left|\mathcal{R}(s,a)-\bar{\mathcal{R}}(\phi(s),a)\right|+\gamma\mathop{\mathbb{E}}_{s,a\sim\xi_{\bar{\pi}}}\left|\mathop{\mathbb{E}}_{s'\sim\mathcal{P}(\cdot|s,a)}V^{\bar{\pi}}(s')-\mathop{\mathbb{E}}_{\bar{s}'\sim\bar{\mathcal{P}}(\cdot|\phi(s),a)}\bar{V}^{\bar{\pi}}(\bar{s}')\right|$$

$$=L_{\mathcal{R}}^{\xi_{\bar{\pi}}}+\gamma\mathop{\mathbb{E}}_{s,a\sim\xi_{\bar{\pi}}}\left|\mathop{\mathbb{E}}_{s'\sim\mathcal{P}(\cdot|s,a)}[V^{\bar{\pi}}(s')-\bar{V}^{\bar{\pi}}(\phi(s'))]+\mathop{\mathbb{E}}_{\substack{\bar{s}'\sim\bar{\mathcal{P}}(\cdot|\phi(s),a)\\s'\sim\mathcal{P}(\cdot|s,a)}}[\bar{V}^{\bar{\pi}}(\phi(s'))-\bar{V}^{\bar{\pi}}(\bar{s}')]\right|$$

$$\leqslant L_{\mathcal{R}}^{\xi_{\bar{\pi}}}+\gamma\mathop{\mathbb{E}}_{s,a\sim\xi_{\bar{\pi}}}\left|\mathop{\mathbb{E}}_{s'\sim\mathcal{P}(\cdot|s,a)}[V^{\bar{\pi}}(s')-\bar{V}^{\bar{\pi}}(\phi(s'))]\right|+\gamma\mathop{\mathbb{E}}_{s,a\sim\xi_{\bar{\pi}}}\left|\mathop{\mathbb{E}}_{\substack{\bar{s}'\sim\bar{\mathcal{P}}(\cdot|\phi(s),a)\\s'\sim\mathcal{P}(\cdot|s,a)}}[\bar{V}^{\bar{\pi}}(\phi(s'))-\bar{V}^{\bar{\pi}}(\bar{s}')]\right|$$

$$\leqslant L_{\mathcal{R}}^{\xi_{\bar{\pi}}}+\gamma\mathop{\mathbb{E}}_{s,a\sim\xi_{\bar{\pi}}}\left|\mathop{\mathbb{E}}_{s'\sim\mathcal{P}(\cdot|s,a)}[V^{\bar{\pi}}(s')-\bar{V}^{\bar{\pi}}(\phi(s'))]\right|+\gamma K_{\bar{V}}\mathop{\mathbb{E}}_{s,a\sim\xi_{\bar{\pi}}}\mathcal{D}\left(\phi\mathcal{P}(\cdot|s,a),\bar{\mathcal{P}}(\cdot|\phi(s),a)\right)$$

$$=L_{\mathcal{R}}^{\xi_{\bar{\pi}}}+\gamma\mathop{\mathbb{E}}_{s,a\sim\xi_{\bar{\pi}}}\left|\mathop{\mathbb{E}}_{s'\sim\mathcal{P}(\cdot|s,a)}[V^{\bar{\pi}}(s')-\bar{V}^{\bar{\pi}}(\phi(s'))]\right|+\gamma K_{\bar{V}}L_{\bar{\mathcal{P}}}^{\xi_{\bar{\pi}}}$$

$$\leqslant L_{\mathcal{R}}^{\xi_{\bar{\pi}}}+\gamma\mathop{\mathbb{E}}_{s,a\sim\xi_{\bar{\pi}}}\mathop{\mathbb{E}}_{s'\sim\mathcal{P}(\cdot|s,a)}\left|[V^{\bar{\pi}}(s')-\bar{V}^{\bar{\pi}}(\phi(s'))]\right|+\gamma K_{\bar{V}}L_{\bar{\mathcal{P}}}^{\xi_{\bar{\pi}}}\text{ Using Jensen's inequality.}$$

$$\leqslant L_{\mathcal{R}}^{\xi_{\bar{\pi}}}+\gamma\mathop{\mathbb{E}}_{s,a\sim\xi_{\bar{\pi}}}\left|[V^{\bar{\pi}}(s)-\bar{V}^{\bar{\pi}}(\phi(s))]\right|+\gamma K_{\bar{V}}L_{\bar{\mathcal{P}}}^{\xi_{\bar{\pi}}}\text{ Applying the stationarity property.}$$

$$\leqslant L_{\mathcal{R}}^{\xi_{\bar{\pi}}}+\gamma\mathop{\mathbb{E}}_{s,a\sim\xi_{\bar{\pi}}}\left|[Q^{\bar{\pi}}(s,a)-\bar{Q}^{\bar{\pi}}(\phi(s),a)]\right|+\gamma K_{\bar{V}}L_{\bar{\mathcal{P}}}^{\xi_{\bar{\pi}}}$$

Solving for the recurrence relation over $\mathbb{E}_{s,a\sim\xi_{\bar{\pi}}}\left|Q^{\bar{\pi}}(s,a)-\bar{Q}^{\bar{\pi}}(\phi(s),a)\right|$ results in the desired result. $\square$

Theorem 6. *Let $\mathcal{M}$ and $\overline{\mathcal{M}}$ be an MDP and a (K_R, K_P)-Lipschitz DeepMDP respectively, with an embedding function ϕ and global loss functions $L_{\mathcal{R}}^{\infty}$ and $L_{\mathcal{P}}^{\infty}$. For all $s \in \mathcal{S}$, the suboptimality of the optimal policy $\bar{\pi}^*$ of $\overline{\mathcal{M}}$ evaluated on $\mathcal{M}$ can be bounded by,*

$$V^*(s)-V^{\bar{\pi}^*}(s)\leqslant 2\frac{L_{\mathcal{R}}^{\infty}+\gamma\left\|\bar{V}^*\right\|_{\mathcal{D}}L_{\mathcal{P}}^{\infty}}{1-\gamma}$$

Where $\left\|\bar{V}^*\right\|_{\mathcal{D}}$ is the smoothness of the optimal value function.

Proof. For any $s \in \mathcal{S}$ we have

$$|V^*(s)-V^{\bar{\pi}^*}(s)|\leqslant|\bar{V}^*(\phi(s))-V^{\bar{\pi}^*}(s)|+|V^*(s)-\bar{V}^*(\phi(s))|. \tag{10}$$

Using the result given by Lemma 7, we may bound the first term of the RHS by $\frac{L_{\mathcal{R}}^{\infty}+\gamma\left\|\bar{V}^*\right\|_{\mathcal{D}}L_{\mathcal{P}}^{\infty}}{1-\gamma}$.

To bound the second therm, we first show that for any $s \in \mathcal{S}, a \in \mathcal{A}$, we have,

$$|Q^*(s,a)-\bar{Q}^*(\phi(s),a)|\leqslant\frac{L_{\mathcal{R}}^{\infty}+\gamma\left\|\bar{V}^*\right\|_{\mathcal{D}}L_{\mathcal{P}}^{\infty}}{1-\gamma}. \tag{11}$$

We prove this similarly to Lemma 2:

$$\sup_{s\in\mathcal{S},a\in\mathcal{A}}\left|Q^*(s,a)-\bar{Q}^*(\phi(s),a)\right| \leqslant \sup_{s\in\mathcal{S},a\in\mathcal{A}}\left|\mathcal{R}(s,a)-\bar{\mathcal{R}}(\phi(s),a)\right| + \gamma\sup_{s\in\mathcal{S},a\in\mathcal{A}}\left|\mathop{\mathbb{E}}_{s'\sim\mathcal{P}(\cdot|s,a)}V^*(s')-\mathop{\mathbb{E}}_{\bar{s}'\sim\bar{\mathcal{P}}(\cdot|\phi(s),a)}\bar{V}^*(\bar{s}')\right|$$

$$= L_{\mathcal{R}}^\infty + \gamma\sup_{s\in\mathcal{S},a\in\mathcal{A}}\left|\mathop{\mathbb{E}}_{s'\sim\mathcal{P}(\cdot|s,a)}[V^*(s')-\bar{V}^*(\phi(s'))] + \mathop{\mathbb{E}}_{\substack{\bar{s}'\sim\bar{\mathcal{P}}(\cdot|\phi(s),a)\\s'\sim\mathcal{P}(\cdot|s,a)}}[\bar{V}^*(\phi(s'))-\bar{V}^*(\bar{s}')]\right|$$

$$\leqslant L_{\mathcal{R}}^\infty + \gamma\sup_{s\in\mathcal{S},a\in\mathcal{A}}\left|\mathop{\mathbb{E}}_{s'\sim\mathcal{P}(\cdot|s,a)}[V^*(s')-\bar{V}^*(\phi(s'))]\right| + \gamma\sup_{s\in\mathcal{S},a\in\mathcal{A}}\left|\mathop{\mathbb{E}}_{\substack{\bar{s}'\sim\bar{\mathcal{P}}(\cdot|\phi(s),a)\\s'\sim\mathcal{P}(\cdot|s,a)}}[\bar{V}^*(\phi(s'))-\bar{V}^*(\bar{s}')]\right|$$

$$= L_{\mathcal{R}}^\infty + \gamma\sup_{s\in\mathcal{S},a\in\mathcal{A}}\left|\mathop{\mathbb{E}}_{s'\sim\mathcal{P}(\cdot|s,a)}[V^*(s')-\bar{V}^*(\phi(s'))]\right| + \gamma\left\|\bar{V}^*\right\|_\mathcal{D}L_{\bar{\mathcal{P}}}^\infty$$

$$\leqslant L_{\mathcal{R}}^\infty + \gamma\max_s\left|V^*(s)-\bar{V}^*(\phi(s))\right| + \gamma\left\|\bar{V}^*\right\|_\mathcal{D}L_{\bar{\mathcal{P}}}^\infty \text{ Using Jensen's inequality.}$$

$$= L_{\mathcal{R}}^\infty + \gamma\max_s\left|\max_a Q^*(s,a)-\max_a\bar{Q}^*(\phi(s),a)\right| + \gamma\left\|\bar{V}^*\right\|_\mathcal{D}L_{\bar{\mathcal{P}}}^\infty$$

$$\leqslant L_{\mathcal{R}}^\infty + \gamma\sup_{s\in\mathcal{S},a\in\mathcal{A}}\left|Q^*(s,a)-\bar{Q}^*(\phi(s),a)\right| + \gamma\left\|\bar{V}^*\right\|_\mathcal{D}L_{\bar{\mathcal{P}}}^\infty$$

Solving for the recurrence gives the desired result. Then, the second therm can be easily bounded:

$$|V^*(s)-\bar{V}^*(\phi(s))| = |\max_a Q^*(s,a)-\max_{a'}\bar{Q}^*(\phi(s),a')| \tag{12}$$

$$\leqslant \max_a|Q^*(s,a)-\bar{Q}^*(\phi(s),a)| \tag{13}$$

$$\leqslant \frac{L_{\mathcal{R}}^\infty + \gamma\left\|\bar{V}^*\right\|_\mathcal{D}L_{\bar{\mathcal{P}}}^\infty}{1-\gamma}. \tag{14}$$

as desired. Combining the bounds for the first and second terms completes the proof. $\square$

B. DonutWorld Experiments

B.1. Environment Specification

Our synthetic environment, DonutWorld, consists of an agent moving around a circular track. The environment is centered at (0,0), and includes the set of points whose distance to the center is between 3 and 6 units away; all other points are out-of-bounds. The distance the agent can move on each timestep is equal to the distance to the nearest out-of-bounds point, capped at 1. We refer to the regions of space where the agent's movements are fastest (between 4 and 5 units away from the origin) as the "track," and other in-bounds locations as "grass". Observations are given in the form of 32-by-32 black-and-white pixel arrays, where the agent is represented by a white pixel, the track by luminance 0.75, the grass by luminance 0.25, and out-of-bounds by black. The actions are given as pairs of numbers in the range (-1,1), representing an unnormalized directional vector. The reward for each transition is given by the number of radians moved clockwise around the center.

Another variant of this environment involves four copies of the track, all adjacent to one another. The agent is randomly placed onto one of the four tracks, and cannot move between them. Note that the value function for any policy is identical whether the agent is on the one-track DonutWorld or the four-track DonutWorld. Observations for the four-track DonutWorld are 64-by-64 pixel arrays.

B.2. Architecture Details

We learn a DeepMDP on states and actions from a uniform distribution over all possible state-action pairs. The environment can be fully represented by a latent space of size two, so that is the dimensionality used for latent states of the DeepMDP.

We use a convolutional neural net for our embedding function ϕ, which contains three convolutional layers followed by a linear transformation. Each convolutional layer uses 4x4 convolutional filters with stride of 2, and depths are mapped to 2,
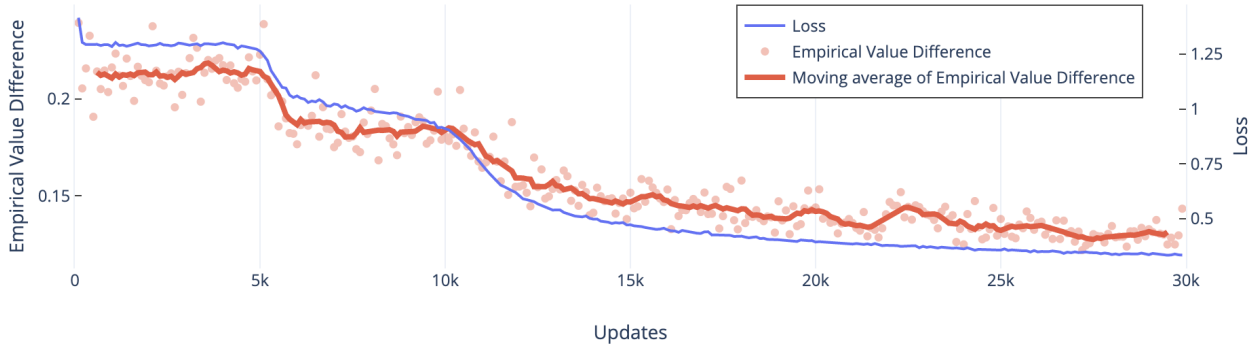
Figure 9. Plot of training curves obtained by learning a DeepMDP on our toy environment. Our objective minimizes both the theoretical upper bound of value difference and the empirical value difference.

then 4, then 8; the final linear transformation maps it to the size of the latent state, 2. ReLU nonlinearities are used between each layer, and a sigmoid is applied to the output to constrain the space of latent states to be bounded by (0, 1).

The transition function and reward function are each represented by feed-forward neural networks, using 2 hidden layers of size 32 with ReLU nonlinearities. A sigmoid is applied output of the transition function.

For the autoencoder baseline, we use the same architecture for the encoder as was used for the embedding function. Our decoder is a three-layer feedforward ReLU network with 32 hidden units per layer. The reconstruction loss is a softmax cross-entropy over possible agent locations.

B.3. Hyperparameters

All models were implemented in Tensorflow. We use an Adam Optimizer with a learning rate of 3e-4, and default settings. We train for 30,000 steps. The batch size is 256 for DMDPs and 1024 for autoencoders. The discount factor, γ, is set to 0.9, and the coefficient for the gradient penalty, λ, is set to 0.01. In contrast to the gradient penalty described in Gulrajani et al. (2017b), which uses its gradient penalty to encourage all gradient norms to be close to 1, we encourage all gradient norms to be close to 0. Our sampling distribution is the same as our training distribution, simply the distribution of states sampled from the environment.

B.4. Empirical Value Difference

Figure 9 shows the loss curves for our learning procedure. We randomly sample trajectories of length 1000, and compute both the empirical reward in the real environment and the reward approximated by performing the same actions in the DeepMDP; this allows us to compute the empirical value error. These results demonstrate that neural optimization techniques are capable of learning DeepMDPs, and that this optimization procedure, designed to tighten theoretical bounds, is minimized by a good model of the environment, as reflected in improved empirical outcomes.

C. Atari 2600 Experiments

C.1. Hyperparameters

For all experiments we use an Adam Optimizer with a learning rate of 0.00025 and epsilon of 0.0003125. We linearly decay epsilon from 1.0 to 0.01 over 1000000 training steps. We use a replay memory of size 1000000 (it must reach a minimum size of 50000 prior to sampling transitions for training). Unless otherwise specified, the batch size is 32. For additional hyperparameter details, see Table 1 and (Bellemare et al., 2017a).

Hyperparameter	Value
`Runner.sticky_actions`	No Sticky Actions
`Runner.num_iterations`	200
`Runner.training_steps`	250000
`Runner.evaluation_steps`	Eval phase not used.
`Runner.max_steps_per_episode`	27000
`WrappedPrioritizedReplayBuffer.replay_capacity`	1000000
`WrappedPrioritizedReplayBuffer.batch_size`	32
`RainbowAgent.num_atoms`	51
`RainbowAgent.vmax`	10.
`RainbowAgent.update_horizon`	1
`RainbowAgent.min_replay_history`	50000
`RainbowAgent.update_period`	4
`RainbowAgent.target_update_period`	10000
`RainbowAgent.epsilon_train`	0.01
`RainbowAgent.epsilon_eval`	0.001
`RainbowAgent.epsilon_decay_period`	100000
`RainbowAgent.replay_scheme`	'uniform'
`RainbowAgent.tf_device`	'/gpu:0'
`RainbowAgent.optimizer`	@tf.train.AdamOptimizer()
`tf.train.AdamOptimizer.learning_rate`	0.00025
`tf.train.AdamOptimizer.epsilon`	0.0003125
`ModelRainbowAgent.reward_loss_weight`	1.0
`ModelRainbowAgent.transition_loss_weight`	1.0
`ModelRainbowAgent.transition_model_type`	'convolutional'
`ModelRainbowAgent.embedding_type`	'conv_layer_embedding'

Table 1. Configurations for the DeepMDP and C51 agents used with Dopamine (Castro et al., 2018) in Section 8.4. Note that the DeepMDP is referred to as ModelRainbowAgent in the configs.

C.2. Architecture Search

In this section, we aim to answer: what latent state space and transition model architecture lead to the best Atari 2600 performance of the C51 DeepMDP? We begin by jointly determining the form of $\bar{\mathcal{S}}$ and $\theta_{\bar{\mathcal{P}}}$ which are conducive to learning a DeepMDP on Atari 2600 games. We employ three latent transition model architectures: (1) single fully connected layer, (2) two-layer fully-connected network, and (3) single convolutional layer. The fully-connected transition networks use the 512-dimensional output of the embedding network's penultimate layer as the latent state, while the convolutional transition model uses the $11 \times 11 \times 64$ output of the embedding network's final convolutional layer. Empirically, we find that the use of a convolutional transition model on the final convolutional layer's output outperforms the other architectures, as shown in Figure 7.

C.3. Architecture Details

The architectures of various components are described below. A conv layer refers to a 2D convolutional layer with a specified stride, kernel size, and number of outputs. A deconv layer refers to a deconvolutional layer. The padding for conv and deconv layers is such that the output layer has the same dimensionality as the input. A maxpool layer performs max-pooling on a 2D input and fully connected refers to a fully-connected layer.

C.3.1. ENCODER

In the main text, the encoder is referred to as $\phi : \mathcal{S} \to \bar{\mathcal{S}}$ and is parameterized by θ_e. The encoder architecture is as follows:

Input: observation s which has shape: batch size $\times 84 \times 84 \times 4$. The Atari 2600 frames are 84×84 and there are 4 stacked frames given as input. The frames are pre-processed by dividing by the maximum pixel value, 255. Output: latent state $\phi(s)$

In Appendix C.2, we experimented with two different latent state representations. (1) *ConvLayer*: The latent state is the
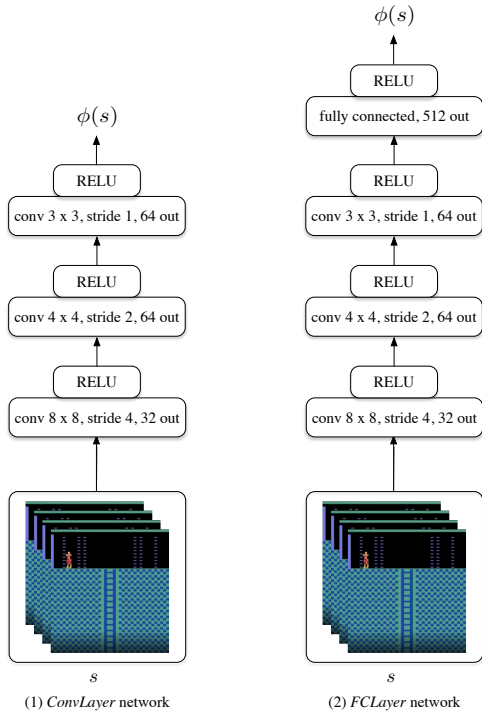
Figure 10. Encoder architectures used for the DeepMDP agent.

output of the final convolutional layer, or (2) *FCLayer*: the latent state is the output of a fully-connected (FC) layer following the final convolutional layer. These possibilities for the encoder architecture are described in Figure 10.

In sections 8.4, 8.5, C.4, and C.5 the latent state of type ConvLayer is used: $11 \times 11 \times 64$ outputs of the final convolutional layer.

C.3.2. LATENT TRANSITION MODEL

In Appendix C.2 there are three types of latent transition models $\bar{\mathcal{P}} : \bar{\mathcal{S}} \to \bar{\mathcal{S}}$ parameterized by $\theta_{\bar{\mathcal{P}}}$ which are evaluated: (1) a single fully-connected layer, (2) a two-layer fully-connected network, and (3) a single convolutional layer (see Figure 11). Note that the first two types of transition models operate on the flattened 512-dimensional latent state (FCLayer), while the convolutional transition model receives as input the $11 \times 11 \times 64$ latent state type ConvLayer. For each transition model, num_actions predictions are made: one for each action conditioned on the current latent state $\phi(s)$.

In sections 8.4, 8.5, C.4, and C.5 the convolutional transition model is used.

C.3.3. REWARD MODEL AND C51 LOGITS NETWORK

The architectures of the reward model $\bar{\mathcal{R}}$ parameterized by $\theta_{\bar{\mathcal{R}}}$ and C51 logits network parameterized by θ_Z depend the latent state representation. See Figure 12 for these architectures. For each architecture type, num_actions predictions are made: one for each action conditioned on the current latent state $\phi(s)$.

In sections 8.4, 8.5, C.4, and C.5 two-layer fully-connected networks are used for the reward and C51 logits networks.

C.3.4. OBSERVATION RECONSTRUCTION AND NEXT OBSERVATION PREDICTION

The models for observation reconstruction and next observation prediction in Section 8.5 are deconvolutional networks based on the architecture of the embedding function ϕ. Both operate on latent states of type ConvLayer. The architectures are described in Figure 13.
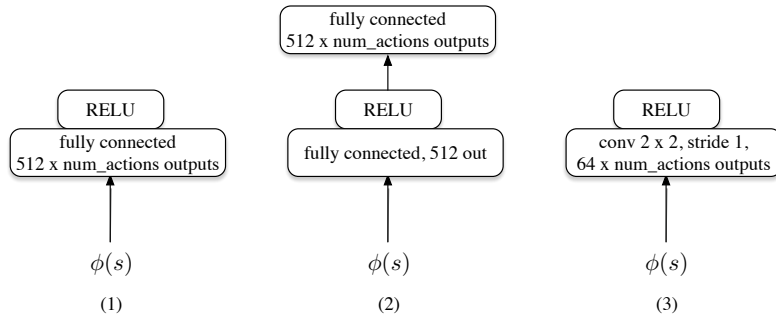
Figure 11. Transition model architectures used for the DeepMDP agent: (1) a single fully-connected layer (used with latent states of type FCLayer), (2) a two-layer fully-connected network (used with latent states of type FCLayer), and (3) a single convolutional layer (used with latent states of type ConvLayer).
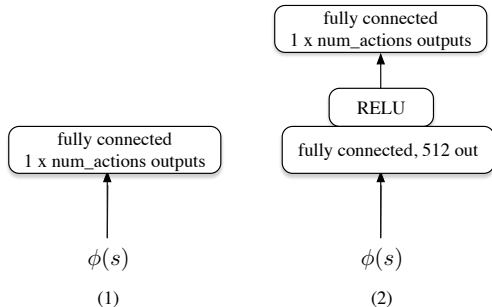

Figure 12. Reward and C51 Logits network architectures used for the DeepMDP agent: (1) a single fully-connected layer (used with latent states of type FCLayer), (2) a two-layer fully-connected network (used with latent states of type ConvLayer).

C.4. DeepMDP Auxiliary Tasks: Different Weightings on DeepMDP Losses

In this section, we discuss results of a set of experiments where we use a convolutional latent transition model and a two-layer reward model to form auxiliary task objectives on top of a C51 agent. In these experiments, we use different weightings in the set $\{0, 1\}$ for the transition loss and for the reward loss. The network architecture is based on the best performing DeepMDP architecture in Appendix C.2. Our results show that using the transition loss is enough to match performance of using both the transition and reward loss. In fact, on Seaquest, using only the reward loss as an auxiliary tasks causes performance to crash. See Figure 14 for the results.

C.5. Representation Learning with DeepMDP Objectives

Given performance improvements in the auxiliary task setting, a natural question is whether optimization of the deepMDP losses is sufficient to perform model-free RL. To address this question, we learn θ_e only via minimizing the reward and latent transition losses. We then learn θ_Z by minimizing the C51 loss but do not pass gradients through θ_e. As a baseline, we minimize the C51 loss with randomly initialized θ_e and do not update θ_e. In order to successfully predict terminal transitions and rewards, we add a terminal reward loss and a terminal state transition loss. The terminal reward loss is a Huber loss between $\overline{\mathcal{R}}(\phi(s_T))$ and 0, where s_T is a terminal state. The terminal transition loss is a Huber loss between $\overline{\mathcal{P}}(s, a)$ and $\mathbf{0}$, where s is either a terminal state or a state immediately preceding a terminal state and $\mathbf{0}$ is the zero latent state.

We find that in practice, minimizing the latent transition loss causes the latent states to collapse to $\phi(s) = 0 \; \forall s \in S$. As (Francois-Lavet et al., 2018) notes, if only the latent transition loss was minimized, then the optimal solution is indeed $\phi : S \to 0$ so that $\overline{\mathcal{P}}$ perfectly predicts $\phi(\mathcal{P}(s, a))$.

We hope to mitigate representation collapse by augmenting the influence of the reward loss. We increase the batch size from 32 to 100 to acquire greater diversity of rewards in each batch sampled from the replay buffer. However, we find that only after introducing a state reconstruction loss do we obtain performance levels on par with our simple baseline. These
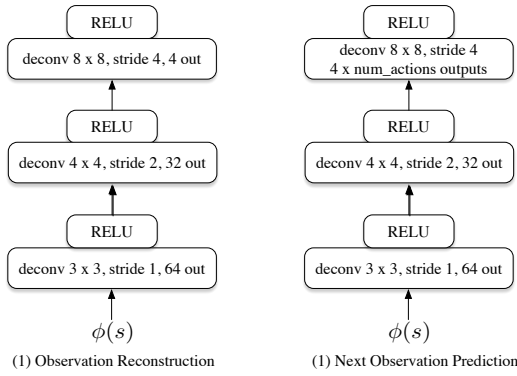
Figure 13. Architectures used for observation reconstruction and next observation prediciton. Both networks take latent states of type ConvLayer as input.
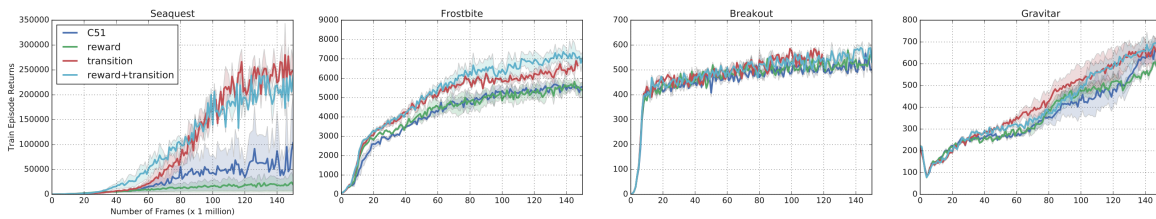

Figure 14. We compare C51 with C51 with DeepMDP auxiliary task losses. The combinations of loss weightings are $\{0, 1\}$ (just reward), $\{1, 0\}$ (just transition), and $\{1, 1\}$ (reward+transition), where the first number is the weight for the transition loss and the second number is the weight for the reward loss.

results (see Figure 15) indicate that in more complex environments, additional work is required to successfully balance the minimization of the transition loss and the reward loss, as the transition loss seems to dominate.

This finding was surprising, since we were able to train a DeepMDP on the DonutWorld environment with no reconstruction loss. Further investigation of the DonutWorld experiments shows that the DeepMDP optimization procedure seems to be highly prone to becoming trapped in local minima. The reward loss encourages latent states to be informative, but the transition loss counteracts this, preferring latent states which are uninformative and thus easily predictable. Looking at the relative reward and transition losses in early phases of training in Figure 5, we see this dynamic clearly. At the start of training, the transition loss quickly forces latent states to be near-zero, resulting in very high reward loss. Eventually, on this simple task, the model is able to escape this local minimum by "discovering" a representation that is both informative and predictable. However, as the difficulty of a task scales up, it becomes increasingly difficult to discover a representation which
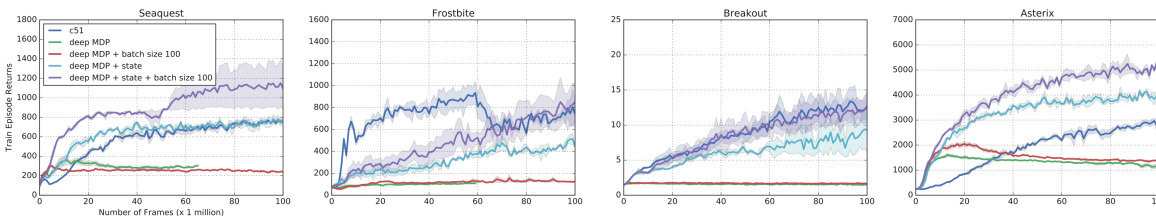

Figure 15. We evaluate the performance of C51 when learning the latent state representation only via minimizing deepMDP objectives. We compare learning the latent state representation with the deepMDP objectives (deep MDP), deepMDP objectives with larger batch sizes (deepMDP + batch size 100), deepMDP objectives and an observation reconstruction loss (deepMDP + state), and deepMDP with both a reconstruction loss and larger batch size (deepMDP + state + batch size 100). As a baselines, we compare to C51 on a random latent state representation (C51).

escapes these local minima by explaining the underlying dynamics of the environment well. This explains our observations on the Arcade Learning Environment; the additional supervision from the reconstruction loss helps guide the algorithm towards representations which explain the environment well.
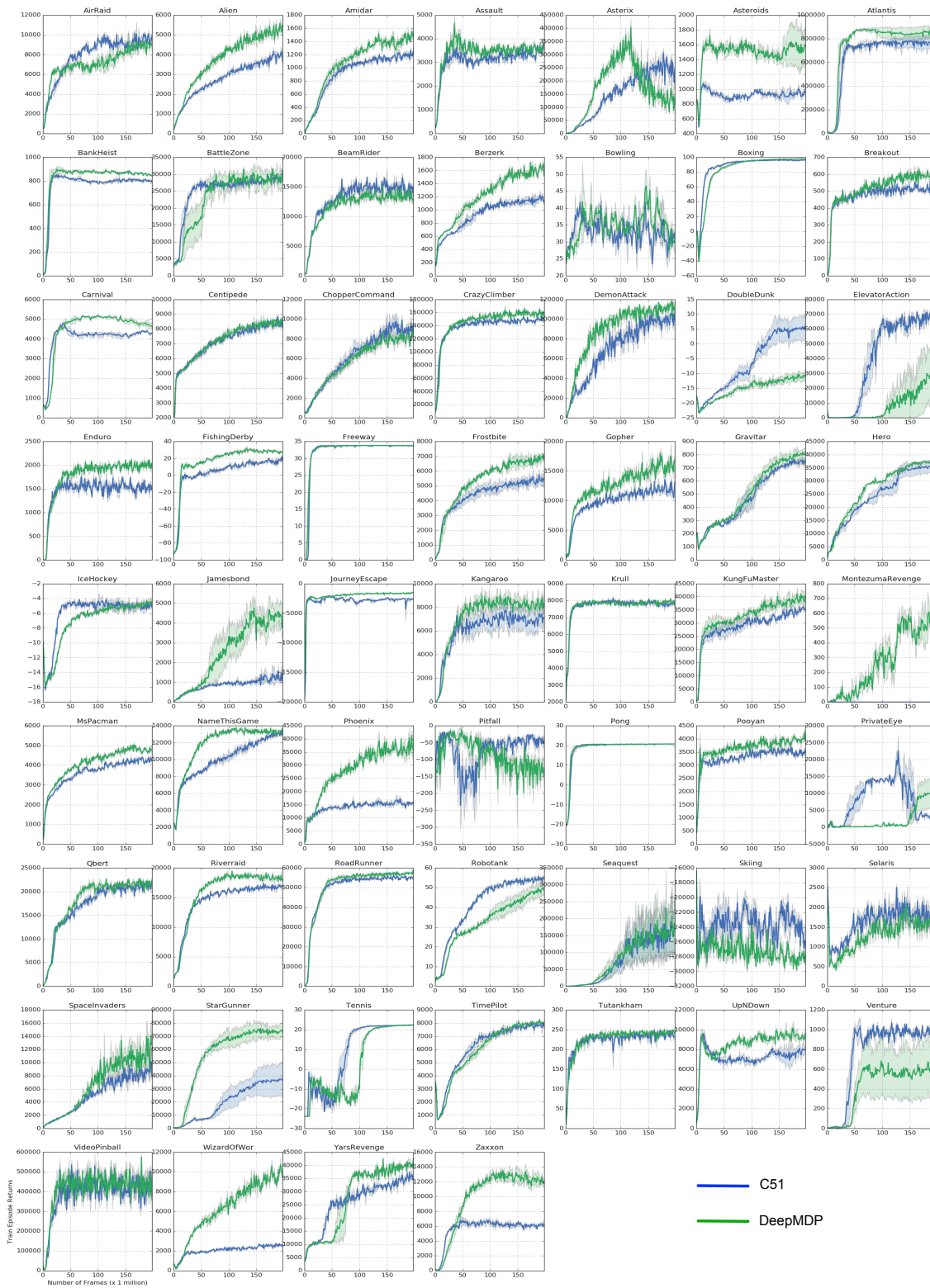
Figure 16. Learning curves of C51 and C51 + DeepMDP auxiliary task objectives (labeled DeepMDP) on Atari 2600 games.

Game Name	C51	DeepMDP
AirRaid	**11544.2**	10274.2
Alien	4338.3	**6160.7**
Amidar	1304.7	**1663.8**
Assault	4133.4	**5026.2**
Asterix	343210.0	**452712.7**
Asteroids	1125.4	**1981.7**
Atlantis	844063.3	**906196.7**
BankHeist	861.3	**937.0**
BattleZone	31078.2	**34310.2**
BeamRider	**19081.0**	16216.8
Berzerk	1250.9	**1799.9**
Bowling	51.4	**56.3**
Boxing	97.3	**98.2**
Breakout	584.1	**672.8**
Carnival	4877.3	**5319.8**
Centipede	**9092.1**	9060.9
ChopperCommand	**10558.8**	9895.7
CrazyClimber	158427.7	**173043.1**
DemonAttack	111697.7	**119224.7**
DoubleDunk	**6.7**	-9.3
ElevatorAction	**73943.3**	37854.4
Enduro	1905.3	**2197.8**
FishingDerby	25.4	**33.9**
Freeway	**33.9**	33.9
Frostbite	5882.9	**7367.3**
Gopher	15214.3	**21017.2**
Gravitar	790.4	**838.3**
Hero	36420.7	**40563.1**
IceHockey	**-3.5**	-4.1
Jamesbond	1776.7	**5181.1**
JourneyEscape	-1856.1	**-1337.1**
Kangaroo	8815.5	**9714.9**
Krull	8201.5	**8246.9**
KungFuMaster	37956.5	**42692.7**
MontezumaRevenge	14.7	**770.7**
MsPacman	4597.8	**5282.5**
NameThisGame	13738.7	**14064.6**
Phoenix	20216.7	**45565.1**
Pitfall	-9.8	**-0.8**
Pong	**20.8**	20.8
Pooyan	4052.7	**4431.1**
PrivateEye	**28694.0**	11223.8
Qbert	23268.6	**23538.7**
Riverraid	17845.1	**19934.7**
RoadRunner	57638.5	**59152.2**
Robotank	**57.4**	51.3
Seaquest	226264.0	**230881.6**
Skiing	**-15454.8**	-16478.0
Solaris	**2876.7**	2506.8
SpaceInvaders	12145.8	**16461.2**
StarGunner	38928.7	**78847.6**
Tennis	22.6	**22.7**
TimePilot	8340.7	**8345.6**
Tutankham	**259.3**	256.9
UpNDown	10175.5	**10930.6**
Venture	**1190.1**	755.4
VideoPinball	**668415.7**	633848.8
WizardOfWor	2926.0	**11846.1**
YarsRevenge	39502.9	**44317.8**
Zaxxon	7436.5	**14723.0**

Table 2. DeepMDP versus C51 returns. For both agents, we report the max average score achieved across all training iterations (each training iteration is 1 million frames).